

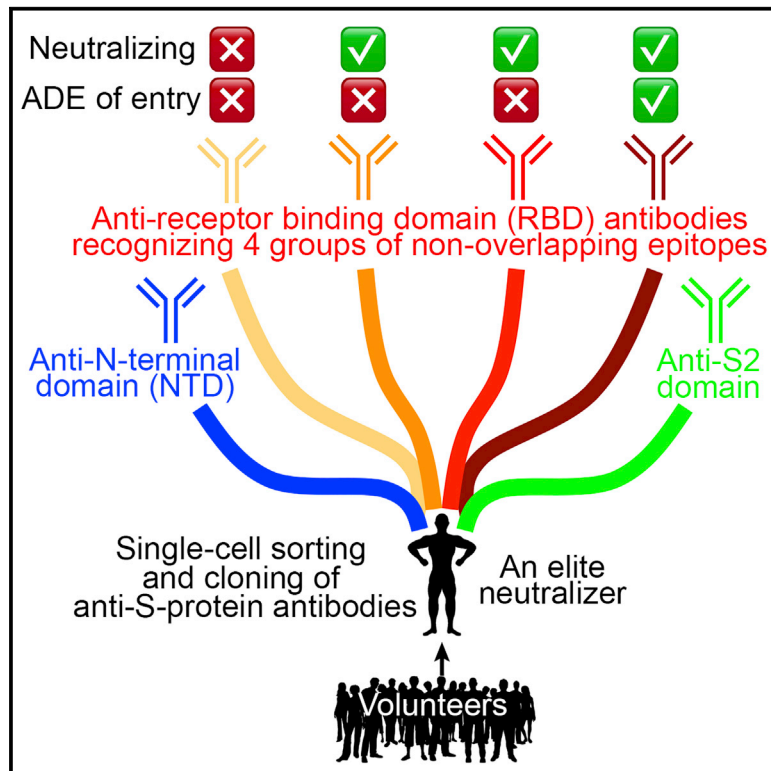


Since January 2020 Elsevier has created a COVID-19 resource centre with free information in English and Mandarin on the novel coronavirus COVID-19. The COVID-19 resource centre is hosted on Elsevier Connect, the company's public news and information website.

Elsevier hereby grants permission to make all its COVID-19-related research that is available on the COVID-19 resource centre - including this research content - immediately available in PubMed Central and other publicly funded repositories, such as the WHO COVID database with rights for unrestricted research re-use and analyses in any form or by any means with acknowledgement of the original source. These permissions are granted for free by Elsevier for as long as the COVID-19 resource centre remains active.

Enhancement versus neutralization by SARS-CoV-2 antibodies from a convalescent donor associates with distinct epitopes on the RBD

Graphical Abstract



Authors

Yunjiao Zhou, Zezhong Liu, Shibo Li, ..., Yumei Wen, Lu Lu, Qiao Wang

Correspondence

zzliu17@fudan.edu.cn (Z.L.), zhyuan@shmu.edu.cn (Z.Y.), yhxie@fudan.edu.cn (Y.X.), ymwen@shmu.edu.cn (Y.W.), lul@fudan.edu.cn (L.L.), wangqiao@fudan.edu.cn (Q.W.)

In Brief

Zhou et al. clone human antibodies against the SARS-CoV-2 S protein from an elite neutralizer and reveal the association of antibody-dependent enhancement (ADE)/neutralizing activities *in vitro* with four distinct groups of non-overlapping epitopes on the receptor-binding domain (RBD).

Highlights

- Antibodies against SARS-CoV-2 S protein are isolated from an elite neutralizer
- Receptor-binding domain (RBD) antibodies target four groups of non-overlapping epitopes
- Group IV antibodies induce antibody-dependent enhancement (ADE) of entry in Raji cells
- Group II/III antibodies neutralize SARS-CoV-2 without mediating ADE of entry *in vitro*



Article

Enhancement versus neutralization by SARS-CoV-2 antibodies from a convalescent donor associates with distinct epitopes on the RBD

Yunjiao Zhou,^{1,9} Zezhong Liu,^{1,9,*} Shibo Li,^{2,9} Wei Xu,^{1,9} Qianqian Zhang,¹ Israel T. Silva,³ Cheng Li,¹ Yanling Wu,¹ Qingling Jiang,⁴ Zhenmi Liu,⁴ Qiujing Wang,² Yu Guo,⁵ Jianbo Wu,¹ Chengjian Gu,¹ Xia Cai,¹ Di Qu,¹ Christian T. Mayer,⁶ Xiangxi Wang,^{7,8} Shibo Jiang,¹ Tianlei Ying,¹ Zhenghong Yuan,^{1,*} Youhua Xie,^{1,*} Yumei Wen,^{1,*} Lu Lu,^{1,*} and Qiao Wang^{1,10,*}

¹Key Laboratory of Medical Molecular Virology (MOE/NHC/CAMS), School of Basic Medical Sciences, Biosafety Level 3 Laboratory, Shanghai Medical College, Fudan University, Shanghai 200032, China

²Department of Infectious Disease, Zhoushan Hospital, Wenzhou Medical University, Zhoushan 316021, China

³Laboratory of Bioinformatics and Computational Biology, A. C. Camargo Cancer Center, São Paulo 01509-010, Brazil

⁴West China School of Public Health and West China Fourth Hospital, Sichuan University, Chengdu 610041, China

⁵State Key Laboratory of Medicinal Chemical Biology and College of Pharmacy, Nankai University, Tianjin 300350, China

⁶Experimental Immunology Branch, Center for Cancer Research, National Cancer Institute, National Institutes of Health, Bethesda, MD 20892, USA

⁷CAS Key Laboratory of Infection and Immunity, National Laboratory of Macromolecules, Institute of Biophysics, Chinese Academy of Sciences, Beijing 100101, China

⁸University of Chinese Academy of Sciences, Beijing 100049, China

⁹These authors contributed equally

¹⁰Lead contact

*Correspondence: zzliu17@fudan.edu.cn (Z.L.), zhyuan@shmu.edu.cn (Z.Y.), yhxie@fudan.edu.cn (Y.X.), ymwen@shmu.edu.cn (Y.W.), lul@fudan.edu.cn (L.L.), wangqiao@fudan.edu.cn (Q.W.)
<https://doi.org/10.1016/j.celrep.2021.108699>

SUMMARY

Several potent neutralizing antibodies against severe acute respiratory syndrome coronavirus 2 (SARS-CoV-2) virus have been identified. However, antibody-dependent enhancement (ADE) has not been comprehensively studied for SARS-CoV-2, and the relationship between enhancing versus neutralizing activities and antibody epitopes remains unknown. Here, we select a convalescent individual with potent IgG neutralizing activity and characterize his antibody response. Monoclonal antibodies isolated from memory B cells target four groups of five non-overlapping receptor-binding domain (RBD) epitopes. Antibodies to one group of these RBD epitopes mediate ADE of entry in Raji cells via an Fc γ receptor-dependent mechanism. In contrast, antibodies targeting two other distinct epitope groups neutralize SARS-CoV-2 without ADE, while antibodies against the fourth epitope group are poorly neutralizing. One antibody, XG014, potently cross-neutralizes SARS-CoV-2 variants, as well as SARS-CoV-1, with respective IC₅₀ (50% inhibitory concentration) values as low as 5.1 and 23.7 ng/mL, while not exhibiting ADE. Therefore, neutralization and ADE of human SARS-CoV-2 antibodies correlate with non-overlapping RBD epitopes.

INTRODUCTION

The ongoing coronavirus disease 2019 (COVID-19) global pandemic is caused by the severe acute respiratory syndrome coronavirus 2 (SARS-CoV-2; also known as 2019-nCoV or HCoV-19) (Coronaviridae Study Group of the International Committee on Taxonomy of Viruses, 2020; Jiang et al., 2020a, 2020c). The four main genera of coronaviruses are known as α , β , γ , and δ . SARS-CoV-2, together with SARS-CoV-1, identified in 2003, and Middle East respiratory syndrome coronavirus (MERS-CoV), identified in 2012, belong to the β -CoV genus (Coronaviridae Study Group of the International Committee on Taxonomy of Viruses, 2020; Zhou et al., 2020; Zhu et al., 2020).

For each coronavirus particle, the viral genome is packed with nucleocapsid (N) proteins and surrounded by an envelope containing structural proteins. One of these structural proteins (spike [S] protein) trimerizes and mediates viral entry into host cells (Li, 2016), and it is the major target for human neutralizing antibodies (Jiang et al., 2020b; Premkumar et al., 2020; Wu et al., 2020a). It contains 1,273 amino acids with a large ectodomain (S-ECD), one transmembrane helix, and a small intracellular C terminus (Figure S1A). Two major domains within S-ECD have been identified as S1 head and S2 stalk regions, and the crucial receptor-binding domain (RBD) localizes to the S1 portion (Figure S1A).

Because binding of SARS-CoV-2 RBD to its human receptor, angiotensin-converting enzyme 2 (ACE2), is a critical initial step



for virus entry into target cells, blocking this interaction with antibodies is likely a promising approach for both treatment and protection. This would be especially true for broadly neutralizing antibodies targeting conserved epitopes present in different coronaviruses, such as SARS-CoV-1 and the newly emerging SARS-CoV-2, both of which are from the same coronavirus subfamily and share the same human receptor ACE2.

Efforts to obtain human neutralizing antibodies against the S protein have involved a variety of methods as phage display (Liu et al., 2020b; Sun et al., 2020; Wu et al., 2020b), humanized mice (Hansen et al., 2020), antibody screening from SARS-CoV-1-recovered individuals (Pinto et al., 2020; Wec et al., 2020), and single B cell antibody cloning from SARS-CoV-2 convalescent donors (Andreano et al., 2020; Brouwer et al., 2020; Cao et al., 2020; Chen et al., 2020; Chi et al., 2020; Ju et al., 2020; Kreer et al., 2020; Liu et al., 2020a; Robbiani et al., 2020; Rogers et al., 2020; Seydoux et al., 2020; Wan et al., 2020; Wu et al., 2020c; Zost et al., 2020a, 2020b). The neutralizing activities of these cloned antibodies are radically different, with 50% inhibitory concentration (IC_{50}) values ranging from single-digit nanograms per milliliter (ng/mL) to non-neutralizing. The antibodies that bind to RBD showed generally higher neutralization potency compared with antibodies with non-RBD epitopes (Rogers et al., 2020). Although some of the reported antibodies showed cross-neutralizing activity (Lv et al., 2020; Pinto et al., 2020; Wec et al., 2020), their potency against SARS-CoV-1 and SARS-CoV-2 was not equally high. Moreover, to the best of our knowledge, the antibody-dependent enhancement (ADE) effect of these antibodies has never been evaluated, and accordingly, the relationship between ADE and different SARS-CoV-2 S protein epitopes has not been determined.

Antibody-bound virus particles could be attached on the surface of immune cells through $Fc\gamma$ -receptor-mediated internalization for subsequent degradation. However, instead of protection, antibody binding might facilitate viral particles to enter and invade host cells. This “ADE of viral entry” phenomenon has been documented for many viruses, including dengue, Zika, and SARS-CoV-1 viruses (Eroshenko et al., 2020; Iwasaki and Yang, 2020; Katzelnick et al., 2017; Miner and Diamond, 2017; Salje et al., 2018). In SARS-CoV-1 infection, antibodies binding the S protein facilitate ACE2-independent virus internalization into macrophages, monocytes, and B cells *in vitro* (Jaume et al., 2011; Wang et al., 2014; Yip et al., 2014). Nevertheless, viral uptake does not necessarily result in a productive viral infection, meaning that ADE of viral entry *in vitro* does not predict ADE of infection and ADE of disease (Arvin et al., 2020; Halstead and Katzelnick, 2020). For example, viral replication was abortive *in vitro* despite enhancement of SARS-CoV-1 virus entry into a B cell line, Raji cells (Jaume et al., 2011). Whether antibodies against SARS-CoV-2 could induce ADE of viral entry and whether the invaded viruses undergo active replication are both still unknown.

Here, we selected a convalescent individual with a high level of serum IgG neutralizing activity against SARS-CoV-2 and isolated many expanded clones of memory B cells expressing closely related antibodies with the same Ig variable gene segments and highly similar CDR3 sequences. Most of these isolated antibodies targeted four groups of five distinct epitopes on the RBD of S protein. Characterization of both neutralizing and enhancing

activities of these antibodies identified an RBD-binding antibody that potently neutralized both SARS-CoV-1 and SARS-CoV-2 and did so without promoting ADE of viral entry. Interestingly, antibodies to one group of RBD epitopes were significantly associated with ADE of entry, while also exhibiting various degrees of neutralization.

RESULTS

Serological responses against SARS-CoV-2

Serum samples were collected from 16 donors who had recovered from SARS-CoV-2 infection and from eight donors before the COVID-19 outbreak (Figure S1B). Compared with the unexposed donors, the sera from recovered individuals displayed significantly higher binding to the SARS-CoV-2 S protein domains (RBD, S1, S2, and S-ECD) by ELISA (Figures 1A–1D; Figure S1A). The N protein within the virion also elicited a robust antibody response after infection (Figure 1E). To determine the neutralizing activity in convalescent sera, we tested their ability to block infection by luciferase-expressing SARS-CoV-2 or SARS-CoV-1 pseudovirus in Huh-7 cells (Xia et al., 2020a, 2020b). The luciferase signal, a surrogate of infection, in the presence of sera or purified IgG antibodies was then compared across a wide range of dilutions (Figures 1F–1H). Although five individuals (donors 5–8 and 16) reached half-maximal neutralizing titers (NT_{50}) above 2,000 for serum samples (Figure 1F), only one individual (donor 16) showed potent neutralization for the purified IgG fraction (NT_{50} : 1.1 μ g/mL; Figure 1H). This discrepancy was possibly due to the neutralizing activities of IgM or IgA antibodies in those convalescent individuals. The serum neutralizing activities of convalescent individuals were much lower against SARS-CoV-1 pseudovirus, yet slightly higher than those in the naive donors (Figure 1G). Thus, all 16 convalescent donors mounted robust antibody responses against SARS-CoV-2 S protein by ELISA, while 5 donors showed high levels of serum neutralizing activities, out of which we selected one for further studies owing to its exceptional serum IgG neutralizing activity.

To determine which domain on the S protein is the dominant target of the neutralizing IgG response in this selected top neutralizer (donor 16), we used RBD, S1, S2, and S-ECD proteins, respectively, to block neutralization *in vitro*. As shown, the IgG neutralizing activity could be partially blocked by RBD, S1, and S-ECD domains, respectively, but not by the S2 domain (Figure 1I). These results suggest that the neutralizing antibody response in donor 16 is directed primarily against the S1 domain and, more specifically, against the RBD within that protein.

Human monoclonal antibodies against SARS-CoV-2 S protein

To characterize the IgG antibodies responsible for the potent neutralizing activity in this selected individual, we identified SARS-CoV-2 RBD- or S-ECD-binding B cells using a dual-dye labeling strategy (Figure S2A) (Wang et al., 2020b). The unexposed naive control showed background levels of bait protein-specific B cells, while donor 16 with high serum neutralizing activity displayed a distinct population of bait protein-binding B cells (Figures 2A–2C). Avi-tagged biotinylated RBD, chemically

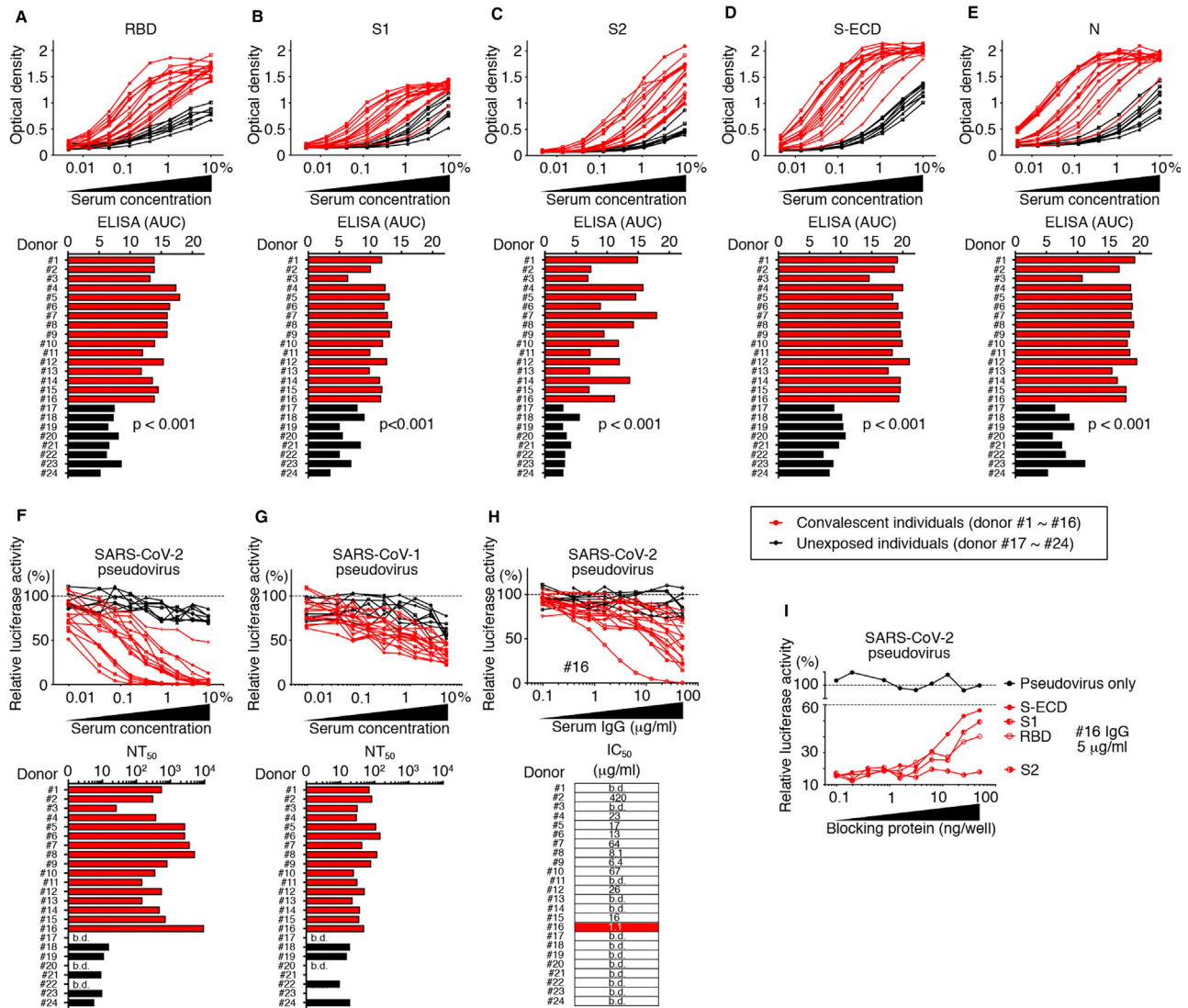


Figure 1. Antibody responses in individuals recovered from SARS-CoV-2 infection

(A–E) ELISA of serum samples. Various sera dilutions from 24 volunteers, including 16 SARS-CoV-2 convalescent individuals (donors 1–16, red lines) and 8 SARS-CoV-2-unexposed naive donors (donors 17–24, black lines), were evaluated by ELISA against SARS-CoV-2 RBD (A), S1 (B), S2 (C), S-ECD (D), and N (E) proteins (upper panel). The area under the ELISA curve (ELISA AUC) values were calculated by PRISM software and presented as columns (bottom panel). The statistical differences (p values) between convalescent and naive donors were determined by Student’s t test for RBD ELISA (A) or by Wilcoxon rank-sum test for others (B–E). A representative of at least two experiments is shown.

(F–H) Luciferase reporter pseudovirus-dependent neutralization assays against SARS-CoV-1 (G) or SARS-CoV-2 pseudovirus (F and H) in the presence of different dilutions of sera (upper panel, F and G) or different concentrations of purified IgG antibodies (upper panel, H). Convalescent individuals are presented in red lines or columns, whereas the unexposed naive donors are in black. The reciprocal of the serum dilution, which resulted in half-maximal inhibition, is reported as the 50% neutralization titer (NT₅₀) and shown as columns (lower panel, F and G). Representative values of the half-maximal inhibitory concentration (IC₅₀) by purified IgG antibodies from at least two independent experiments are shown (lower panel, H). Colored shading indicates the most inhibitory samples from donor 16.b.d., below detection.

(I) Blocking of neutralization by different S protein domains. Different amounts of the indicated proteins (RBD, S1, S2, and S-ECD of SARS-CoV-2 S protein) were incubated with purified polyclonal IgG (5 μg/mL from donor 16, red lines) before incubation with SARS-CoV-2 pseudovirus for *in vitro* infection. Infection efficiency by SARS-CoV-2 pseudovirus alone is shown as a black line. y axis shows normalized luciferase reading values as an indicator of infection efficiency.

See also Figure S1.

biotinylated S-ECD, and Avi-tagged biotinylated S-ECD bait proteins stained B cells at a frequency of 0.025%, 0.12%, and 0.21%, respectively, which were about 6- to 20-fold over that of background staining (Figures 2A–2C).

The gated double-positive cells (bait protein-phycoerythrin positive [PE⁺] and bait protein-allophycocyanin positive [APC⁺]) were single cell sorted, and immunoglobulin heavy (*IgH*; IgG isotype) and light (*IgL* or *IgK*) chain genes were amplified by nested PCR

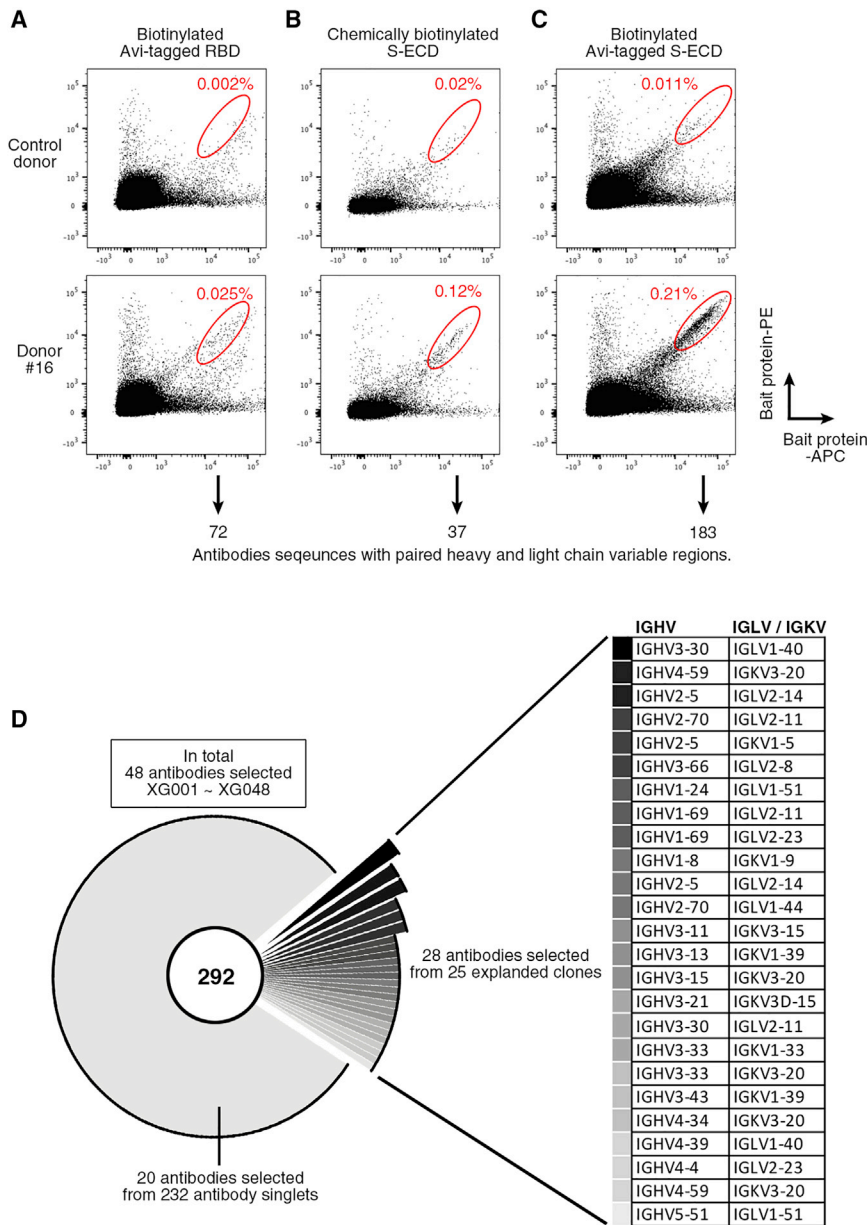


Figure 2. Cloning of S protein-specific antibodies

(A–C) Frequency of B lymphocytes recognizing SARS-CoV-2 proteins in naive control donor (upper panel) and selected donor 16 (lower panel). Representative flow cytometry plots displaying the percentage of CD19⁺ CD20⁺ B cells that bind to biotinylated Avi-tagged RBD (A), chemically biotinylated S-ECD (B), and biotinylated Avi-tagged S-ECD (C). All bait proteins were labeled with either allophycocyanin (APC) or phycoerythrin (PE) for a two-fluorescent-dye sorting strategy (Figure S2A). Experiments were repeated at least two times.

(D) Antibody pie chart for donor 16. There are in total 292 sequenced antibodies with naturally paired Ig heavy and light chains. Antibodies with the same combination of IGH and IGL variable gene sequences and closely related CDR3s were grouped together and represented as a slice. In total, 25 slices were identified, and IGHV and IGKV/IGLV genes are shown for each slice (see more details in Table S1). Antibody singlets are in one big silver slice. In total, 48 monoclonal antibodies (XG001–XG048) were selected for further characterization.

See also Figure S2 and Table S1.

Antibody epitopes

In total, 48 antibodies, designated as XG001 to XG048, were selected for expression and further characterization: 28 from 25 expanded clones and 20 from singlets (Figure 2D; Table S1). 45 of 48 antibodies (94%) showed reactivity to the SARS-CoV-2 S-ECD protein (non-binders: gray name, Figure 3A), and 23 of 48 (48%) antibodies showed RBD binding capacity (red name, Figure 3B). All of these RBD-binding antibodies showed ELISA binding against the S1 domain, as expected (Figures 3B and 3C). An additional 11 antibodies with no RBD binding (23%) also bound to the S1 domain (blue name, Figure 3C), suggesting reactivity to the N-terminal domain (NTD), as previously reported

(Robbiani et al., 2017; Scheid et al., 2009; Wang et al., 2020b). Overall, we obtained 292 paired heavy and light chain variable regions from RBD-binding and S-ECD-binding IgG⁺ memory B cells (Figure 2D; Table S1). Sequence analysis showed a broad spectrum of immunoglobulin heavy chain V gene (IGHV) usage, CDRH3 amino acid length distribution, and mutation frequency (Figures S2B–S2D). Moreover, 25 expanded clones producing antibodies encoded by the same Ig variable gene segments with closely related CDR3 sequences were identified (Figure 2D; Table S1). The antibodies from the same clones showed 80% or higher similarities at the amino acid level (Figure S2E). We conclude that this SARS-CoV-2 neutralizer, similar to other reported donors (Cao et al., 2020; Kreer et al., 2020; Robbiani et al., 2020), produced clones of antigen-binding memory B cells that express related Ig heavy and light chains.

(Chi et al., 2020). We also found 5 of 48 antibodies (10%) that bound to the S2 domain (green name, Figure 3D). Moreover, 6 of 48 antibodies (12%) with no or only weak binding to S1/S2/RBD proteins showed S-ECD binding affinity (purple name, Figures 3A–3D), implying that these antibodies recognize epitopes not present or altered in separate domains. In summary, the selected 48 antibodies from this volunteer recognize various epitopes on the SARS-CoV-2 S protein, and almost half of them bind to the RBD (Figure 3E).

To further determine whether the RBD-binding antibodies bind to overlapping or non-overlapping epitopes, we performed competition ELISAs. Antibodies with weak levels of ELISA binding (XG010, XG015, XG042, XG045, XG047) were excluded. The coated RBD protein was first pre-incubated with a

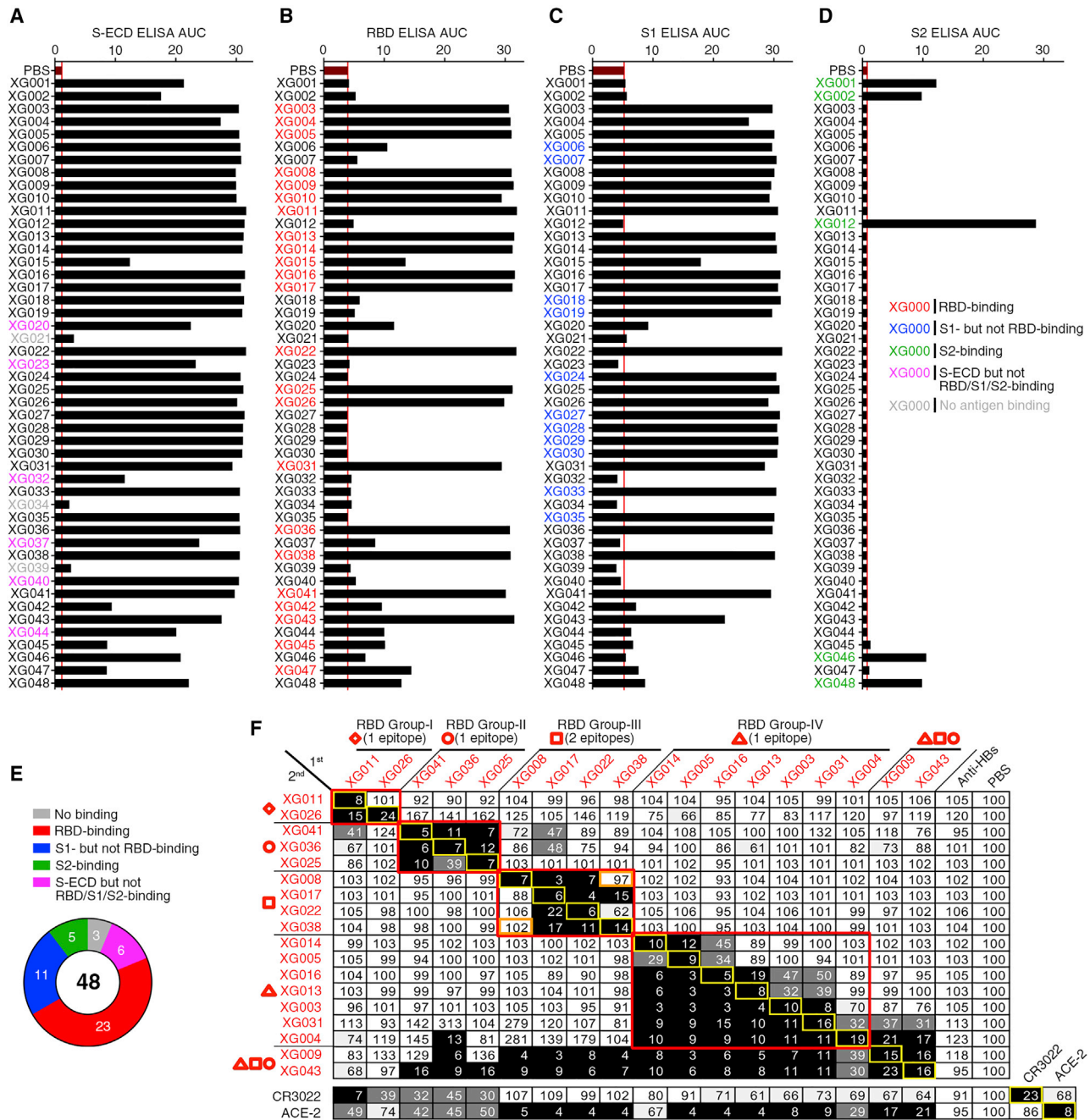


Figure 3. Antibody epitopes within the SARS-CoV-2 S protein

(A–D) Binding of human monoclonal antibodies to different domains of the SARS-CoV-2 S protein. The representative area under the curve (AUC) values for ELISAs using S-ECD (A), RBD (B), S1 (C), and S2 (D) from at least two independent experiments are shown. Phosphate-buffered saline (PBS) was used as a negative control.

(E) Based on antigen-binding assays, 48 antibodies were categorized into five types: red, RBD-binding antibodies; blue, S1- but not RBD-binding antibodies; green, S2-binding antibodies; purple, S-ECD- but not RBD/S1/S2-binding antibodies; and gray, no binding on the tested antigens. The names of monoclonals in (A)–(D) are color coded correspondingly.

(F) A competition ELISA defines four non-overlapping epitope groups (four symbols with the corresponding red rectangles) and a fifth overlapping epitope group (XG009 and XG043, overlapping with group II–IV antibodies) of RBD-binding antibodies. The first antibodies/proteins (x axis) were non-biotinylated and used to block the epitopes, whereas the second antibodies/proteins (y axis) were biotinylated for detection by streptavidin-horseradish peroxidase (HRP). Results of competition ELISA are shown as percent of binding by the second biotinylated antibodies compared with PBS-blocked references and are illustrated by colors: black, 0%–25%; dark gray, 25%–50%; light gray, 50%–75%; and white, >75%. All of the tested antibodies blocked the binding of their own biotinylated versions (legend continued on next page)

non-biotinylated first antibody followed by incubation with a second biotinylated antibody. As expected, all of the tested antibodies competed with themselves (yellow rectangles, Figure 3F), while control antibody anti-HBs H004 (Wang et al., 2020b) failed to block any of the RBD antibodies (Figure 3F). In the RBD (amino acid 330–530), four mutually exclusive groups of antibodies (groups I–IV) were identified by the competition ELISAs (red rectangles, Figure 3F). Further competition ELISA assays showed that the epitope of monoclonal antibody CR3022 (ter Meulen et al., 2006) overlapped with group I and II, but not group III and IV, antibodies (Figure 3F). Moreover, the binding of ACE2 was efficiently blocked by all of the tested antibodies (Figure 3F), except three monoclonals: CR3022, consistent with a previous report (Tian et al., 2020); a non-neutralizing antibody, XG026; and a potentially neutralizing antibody, XG014.

In group III, although antibodies XG017 and XG022 blocked the binding of XG008 and XG038, the latter two antibodies bound non-competitively to RBD (two orange boxes, Figure 3F). Thus, among group III antibodies, we had found two mutually exclusive sub-epitopes. This was further confirmed by showing that a combination of four antibodies recognizing distinct epitopes could not block the binding of the fifth antibody to either RBD or S-ECD proteins (Figures S3A–S3C). Moreover, antibodies in each RBD group have different IGHV and IGKV/IGLV usage (Figure S3D). Besides the four groups of non-overlapping antibodies against SARS-CoV-2 RBD, two antibodies, XG009 and XG043, competed across groups (Figure 3F), which could be interpreted by their binding mode bridging all these epitopes or by altered antigen conformation induced by antibody binding. Together, these results indicate that there are at least four groups comprising five non-overlapping antibody-binding epitopes on the RBD of SARS-CoV-2.

SARS-CoV-2 neutralizing activity *in vitro*

To determine whether our selected antibodies block SARS-CoV-2 infection *in vitro*, we performed neutralization assays using luciferase-expressing SARS-CoV-2 pseudoviruses to infect Huh-7 cells (Xia et al., 2020a, 2020b) and calculated their IC₅₀ values (Figures 4A and 4B). The neutralizing activity of these antibodies varied dramatically, ranging from potent neutralizers to non-neutralizing. Among the 48 tested antibodies, almost half of them (23 antibodies) showed neutralizing activities with IC₅₀ values lower than 10 μg/mL, while 7 of them were the most potent with IC₅₀ values lower than 0.1 μg/mL (Figure 4C). These neutralizing antibodies recognized distinct epitopes, including RBD, S2, or other non-RBD domains. Similar to other studies (Premkumar et al., 2020; Rogers et al., 2020), most of our cloned monoclonals with neutralizing activity bound S protein RBD (Figure 4C). The most potent antibodies displayed IC₅₀ values of 6–15 ng/mL, with four of them being RBD binding, including XG005 (IC₅₀: 6.1 ng/mL), XG014 (IC₅₀: 14.4 ng/mL), XG016 (IC₅₀: 9.1 ng/mL), and XG038 (IC₅₀: 12.7 ng/mL), and one of

them being S1 binding, but not RBD binding, namely, XG027 (IC₅₀: 15.7 ng/mL) (Figures 4A and 4B).

We then chose several monoclonals (XG005, XG008, XG013, XG014, XG016, XG017) to confirm their neutralizing activities using authentic SARS-CoV-2 virus (Figures 4D–4F; Figure S4). Infectivity was quantified using immunofluorescence by anti-N protein polyclonal antibodies (Figure 4D; Figure S4), as well as quantitative reverse transcription PCR of the culture medium (Figure 4E). Results were consistent across these two readouts and showed that these antibodies were potent neutralizers against authentic SARS-CoV-2 viruses, with IC₅₀ values as low as single-digit ng/mL, such as XG014 (IC₅₀: 5.1 ng/mL) (Figures 4E and 4F). Compared with SARS-CoV-2 pseudovirus, some monoclonals, such as XG017, showed significantly more neutralizing activities against authentic SARS-CoV-2 viruses, whereas others, including XG005 and XG016, had reduced effects (Figures 4B and 4F). We conclude that several isolated monoclonal antibodies, such as RBD-binding antibodies XG014 and XG017, could potentially neutralize authentic SARS-CoV-2 virus *in vitro*.

To determine the relationship between the neutralizing activity of monoclonals and their binding epitopes, we performed unsupervised hierarchical clustering using the nine normalized luciferase values from neutralization assays with their corresponding epitope labeled (Figure 4G). Antibody clusters A–D with different levels of neutralizing activity were identified. Compared with non-neutralizing antibodies in cluster D, antibodies in clusters A and B, most of which are against RBD group II–IV epitopes, were potent neutralizers, whereas antibodies in cluster C were weakly neutralizing antibodies (Figure 4G). Antibodies targeting the RBD group I epitope were barely neutralizing in our assays (Figure 4G). Therefore, potent neutralizing antibodies target some, but not all, RBD epitopes.

Cross-neutralizing activity against SARS-CoV-2 RBD mutants and SARS-CoV-1

Point mutations in MERS-CoV and SARS-CoV-1 have been demonstrated to confer resistance to naturally occurring neutralizing antibodies (Sui et al., 2008; Tang et al., 2014; ter Meulen et al., 2006). The pandemic SARS-CoV-2 virus is also slowly mutating (Korber et al., 2020; Li et al., 2020). Thus, monitoring the single amino acid changes and understanding their underlying phenotypical relevance are crucial. To extract more structural information about the location of antibody epitopes and to assess antibody responses against escape mutations, we performed ELISA assays using 32 RBD mutants, including 25 naturally occurring mutants and 7 alanine mutants (F377A, S383A, P384A, T385A, K386A, L390A, and D428A) (Figure 5A). Comparing with the binding to wild-type RBD, group I and IV, but not group II and III, antibodies showed reduced binding activity to RBD mutant L390A (Figures 5A and 5B). Neutralizing

(yellow rectangles). XG008 and XG038 bind two mutually exclusive sub-epitopes (orange rectangles) in RBD group III. Anti-HBs antibody H004 (Wang et al., 2020b) was used as negative control. Monoclonal antibody CR3022 (ter Meulen et al., 2006) and recombinant ACE2 protein (Wu et al., 2020b) were used for mapping the epitopes of our cloned antibodies. Weak RBD binders (XG015, XG042, XG045, and XG047) were excluded in this assay. Representative of two experiments.

See also Figure S3.

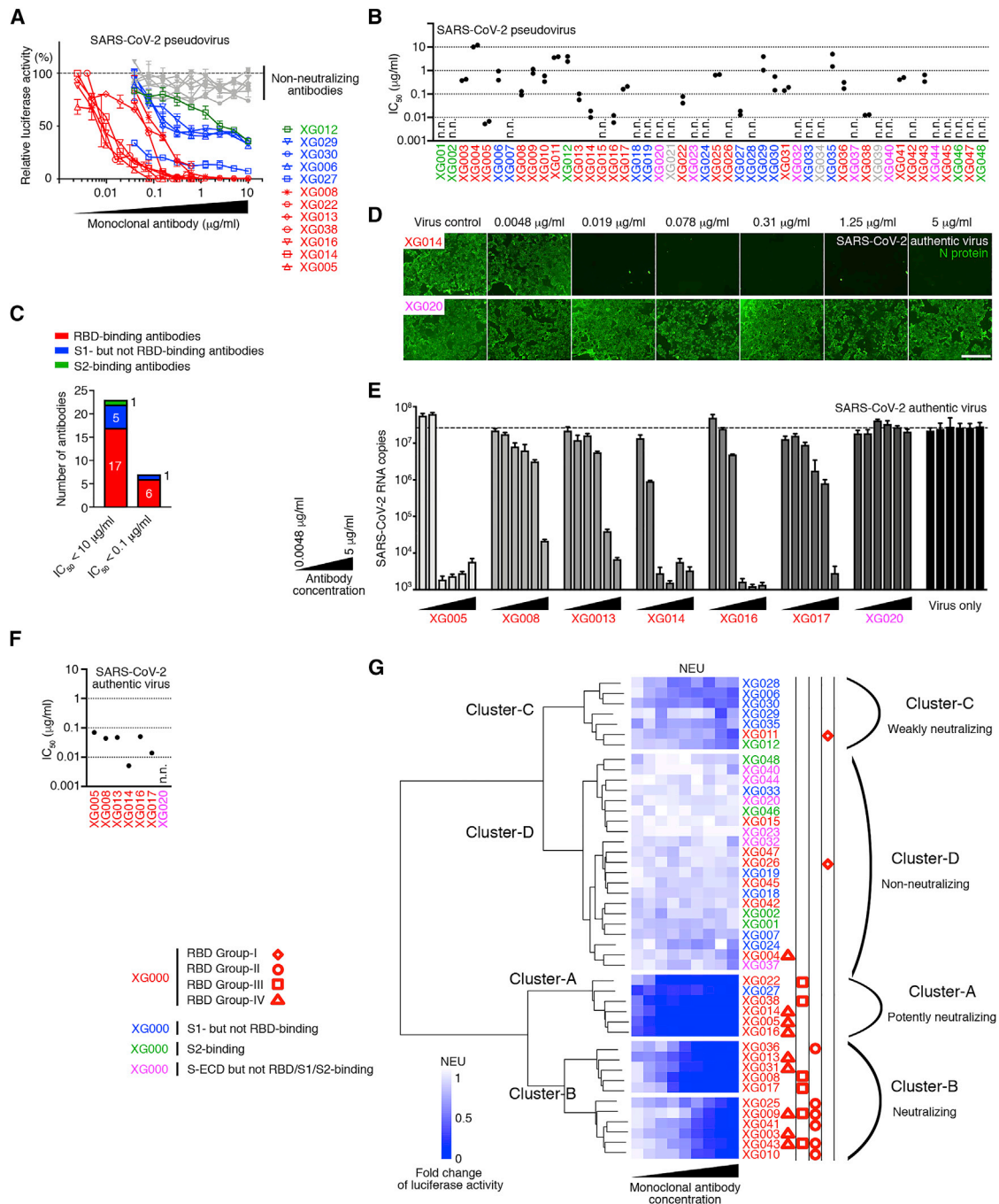


Figure 4. In vitro neutralization activity

(A) Neutralization potency of representative human monoclonal antibodies using luciferase-based SARS-CoV-2 pseudovirus. The luciferase signal (a surrogate of infection) was determined in the presence of various concentrations of monoclonals as indicated and normalized to the no antibody control (dashed line). Tested antibodies with no neutralizing capacities in our assays are shown in gray lines, while antibodies against distinct epitopes, RBD (red), S1, but not RBD (blue), or S2 (green), are shown in different colors. Duplicates of neutralization are presented as mean \pm range.

(B) The IC_{50} values for each antibody determined by *in vitro* neutralization assays against SARS-CoV-2 pseudovirus are shown. All experiments were repeated a minimum of two times. n.n., not neutralizing in our assays. Different colors for the names of monoclonal antibodies represent different antigen-epitopes (see more details in Figure 3E).

(C) The antigen epitopes of neutralizing antibodies with IC_{50} lower than 10 or 0.1 µg/mL are summarized in columns.

(legend continued on next page)

antibodies XG022, XG017, XG008, XG014, XG005, and XG025 exhibited resistance to most mutations (Figure 5A).

To test the possibility that some of these mutations might be acquired in order to confer antibody resistance, we picked two monoclonals, XG014 and XG038, for neutralization assays against several SARS-CoV-2 pseudoviruses carrying some of these reported RBD mutations, such as V341I, F342L, V367F, R408I, A435S, G476S, and V483A (Figure 5B). All SARS-CoV-2 variants tested remained sensitive to XG014 (Figure 5C), while two of the seven viruses showed resistance to XG038 antibody neutralization (G476S and V483A; Figure 5D). This result is consistent with the ELISA result that XG038 exhibited reduced binding activity to these two RBD mutants (G476S and V483A; Figure 5A). Therefore, some RBD point mutations can confer SARS-CoV-2 resistance to some human neutralizing antibodies.

To further determine the breadth of our cloned monoclonal antibodies, we measured their neutralizing activity against SARS-CoV-1 pseudoviruses *in vitro*. XG014 and XG041 could neutralize SARS-CoV-1 pseudovirus *in vitro*, with IC₅₀ values of 23.7 and 1,140 ng/mL, respectively (Figures 5E and 5F; Figure S5). None of the other antibodies showed neutralizing activity against SARS-CoV-1 pseudovirus in our assays (Figure 5E). Thus, SARS-CoV-2 infection can generate rare cross-neutralizing antibodies, such as XG014, which potently neutralize SARS-CoV-1 and SARS-CoV-2, as well as SARS-CoV-2 RBD mutants.

ADE

Although antibodies can clear viruses or infected cells through its binding to Fc γ receptors on host immune cells, these interactions could also lead to disease enhancement during coronavirus infection (Eroshenko et al., 2020; Iwasaki and Yang, 2020). Determination of ADE effect would be a crucial step for the clinical use of potent neutralizing antibodies. Raji cells, originally derived from a Burkitt's lymphoma patient, have been shown to facilitate SARS-CoV-1 infection in the presence of anti-S protein immune serum (Jaume et al., 2011). Thus, we used this Fc γ R1I-bearing human B lymphoblast cell line to study the antibody-dependent viral entry (ADE of viral entry) of SARS-CoV-2 *in vitro* as an indicator of ADE.

No infection of Raji cells was detected by luciferase-expressing SARS-CoV-2 pseudovirus alone or in the presence of different concentrations of human serum samples collected from healthy donors or convalescent individuals (Figure S6A). We then measured the antibody-dependent entry of SARS-CoV-2 pseudoviruses in the presence of monoclonals. Eleven of 48 antibodies (23%) significantly enhanced viral infection of Raji cells, while no viral infection was induced by the remaining antibodies, including the two most potent neutralizers, XG014

and XG038 (Figure 6A; Figure S6B). Among the 11 enhancing antibodies, 9 were RBD-binding antibodies, and 2 antibodies bound to S1, but not RBD (Figure 6B). No S2-binding antibodies induced Raji cell infection. Monoclonal antibodies induced different patterns of infection. For example, XG006 enhanced only infection of Raji cells when present at high concentrations, but lost the enhancement effect when diluted, whereas XG005 induced viral infection at all dilutions tested (Figure 6A; Figure S6B). ADE area under the curve (AUC) and the enhancing power (see the definitions in Figure S6C) were calculated as previously reported (Bardina et al., 2017; Robbiani et al., 2019) (Figure 6C; Figure S6D), and a positive correlation was observed between these two values (Figure S6E). However, no significant correlation was observed between the calculated IC₅₀ values of neutralization and the corresponding ADE AUC or enhancing power values (Figures S6F and S6G).

Antibody-dependent viral entry was fully abrogated by GRLR mutations G236R and L328R (Horton et al., 2008) in the antibody Fc receptor binding site (Figures 6D and 6E). A similar effect was also achieved by incubating the cells with anti-Fc γ R1I antibodies (Figure 6F), further demonstrating the requirement of Fc γ receptor binding for antibody-dependent SARS-CoV-2 viral entry. Therefore, some SARS-CoV-2 anti-RBD and anti-S1 antibodies induce ADE of viral entry in Raji cells through the Fc γ receptor-dependent mechanism.

To examine whether such an ADE effect could also be seen with authentic SARS-CoV-2 virus, we infected Raji cells with authentic SARS-CoV-2 virus in the presence of different monoclonals. Similar to phosphate-buffered saline (PBS), only the background level of viral RNA was detected in the presence of non-ADE antibody XG038 (Figure 6G). ADE antibodies, XG005 and XG016, induced higher levels of cellular viral load, especially after 24 h of incubation (Figure 6G), suggesting that the ADE of viral entry by authentic SARS-CoV-2 virus in immune cells is similar to that observed with pseudovirus. Moreover, the low level of viral RNA detected in the cells after 6-h incubation suggested that a longer period of incubation is required for antibody-mediated viral entry *in vitro* (Figure 6G). However, compared with those after 24-h incubation, a decreased level of viral RNA after 48-h incubation (Figure 6G) is similar to the abortive SARS-CoV-1 infection previously reported (Jaume et al., 2011). Taken together, despite the ability of SARS-CoV-2 virus for ADE of viral entry, no significant viral replication was detected in Raji cells.

Association of antibody properties and epitopes

Clinically, it would be imperative to segregate antibodies based on a combination of functional features. Accordingly, we

(D) Immunofluorescent staining of SARS-CoV-2 N protein for *in vitro* neutralization assays against authentic SARS-CoV-2 virus. Immunofluorescence using anti-N protein polyclonal antibodies (Gu et al., 2020) was used to evaluate the neutralizing effect of selected monoclonals. Non-neutralizing antibody XG020 was used as a negative control. Scale bar, 400 μ m. Immunofluorescent and DAPI staining figures of other monoclonals are shown in Figure S4.

(E and F) Quantitative reverse transcription PCR results (E) and the corresponding IC₅₀ values (F) for *in vitro* neutralization assays against authentic SARS-CoV-2 virus. SARS-CoV-2 N protein RNA copy numbers were calculated using a standard curve composed of seven prepared N protein DNA samples with 10-fold serial dilutions. At least two independent experiments were performed.

(G) Clustering analysis identified antibody epitopes associated with neutralizing activity. Unsupervised hierarchical clustering was performed using the SARS-CoV-2 pseudovirus neutralization data in the presence of nine dilutions of 45 monoclonals. Clusters A–D were identified. Antibodies with no ELISA binding against our tested antigens (XG021, XG034, XG039) were excluded. Antibodies with different epitopes on the S protein or RBD are color or shape coded, respectively. See also Figure S4.

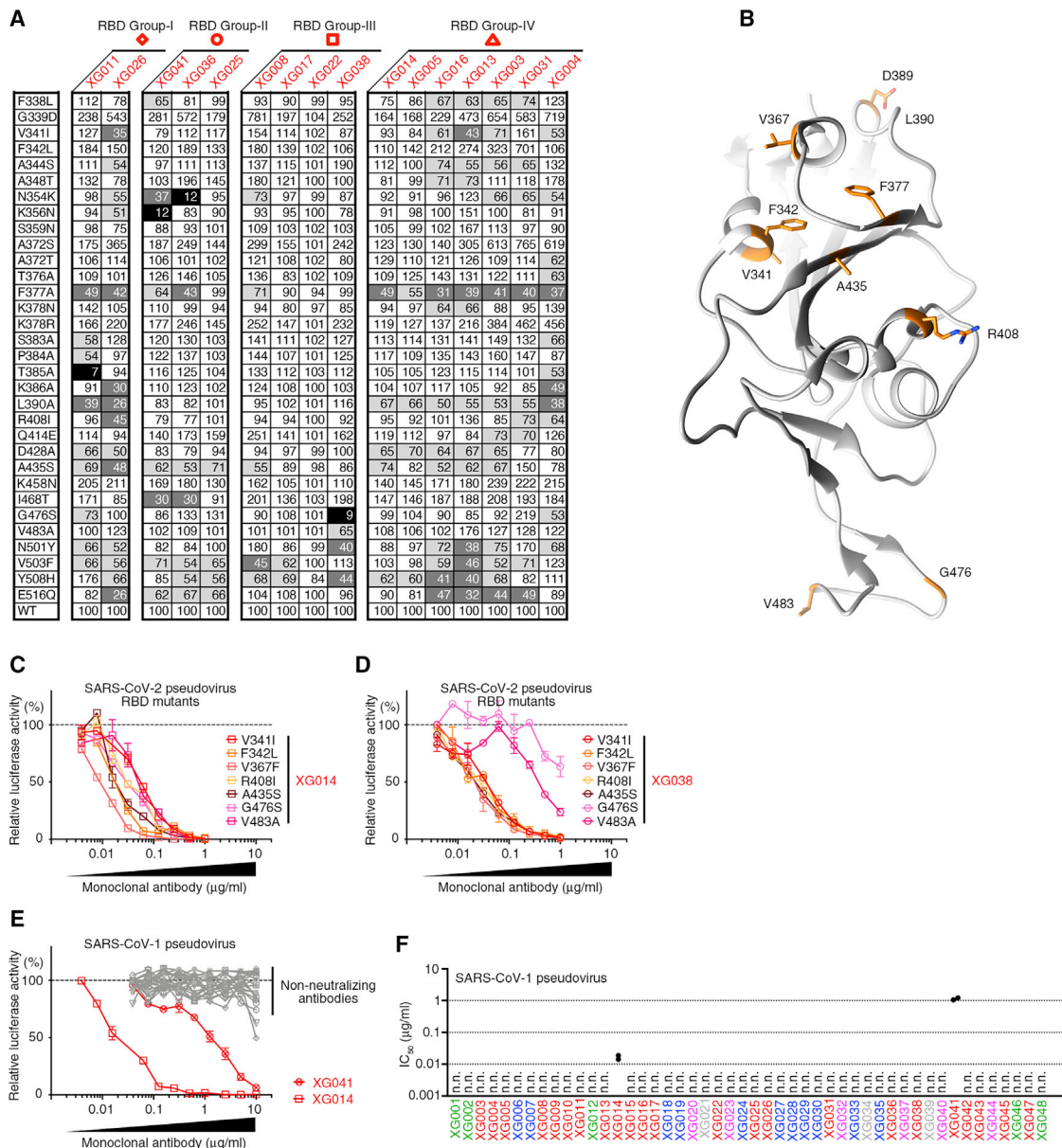


Figure 5. Cross-neutralizing activity by monoclonal antibodies

(A) ELISA assays using various RBD mutants. Group I–IV antibodies were tested for their binding activities to 32 different recombinant RBD mutants, including 25 naturally occurring mutants and 7 artificially generated alanine mutants (F377A, S383A, P384A, T385A, K386A, L390A, and D428A). The binding capacities are shown as percent of binding to wild-type RBD and are illustrated by colors: black, 0%–25%; dark gray, 25%–50%; light gray, 50%–75%; white, >75%.

(B) Structure diagram of SARS-CoV-2 RBD (PDB: 6W41, crystal structure of SARS-CoV-2 RBD) (Yuan et al., 2020) with several positions of the tested mutations marked.

(C and D) *In vitro* neutralization assays of XG014 (C) and XG038 (D) against SARS-CoV-2 pseudoviruses with distinct RBD mutations. Luciferase activity was determined, normalized, and considered as a surrogate of infection. The reference used for normalization had no antibody added (dashed line), and duplicates of neutralization are presented as mean ± range.

(E and F) *In vitro* neutralization experiments against SARS-CoV-1 pseudovirus (E) and the corresponding IC₅₀ values for each antibody (F). n.n., not neutralizing in our assays. Tested antibodies with no neutralizing capacities in our assays are shown in gray lines in (E). At least two experiments were performed, and duplicates of neutralization are presented as mean ± range.

See also Figure S5.

performed unsupervised hierarchical clustering using the nine normalized luciferase values from both neutralization assays and the ADE assays. Three major antibody clusters (clusters X,

Y, and Z) were identified (Figure 7A). Cluster X antibodies were characterized by having both neutralizing and enhancing activities. Cluster Y antibodies displayed potent neutralizing activity,

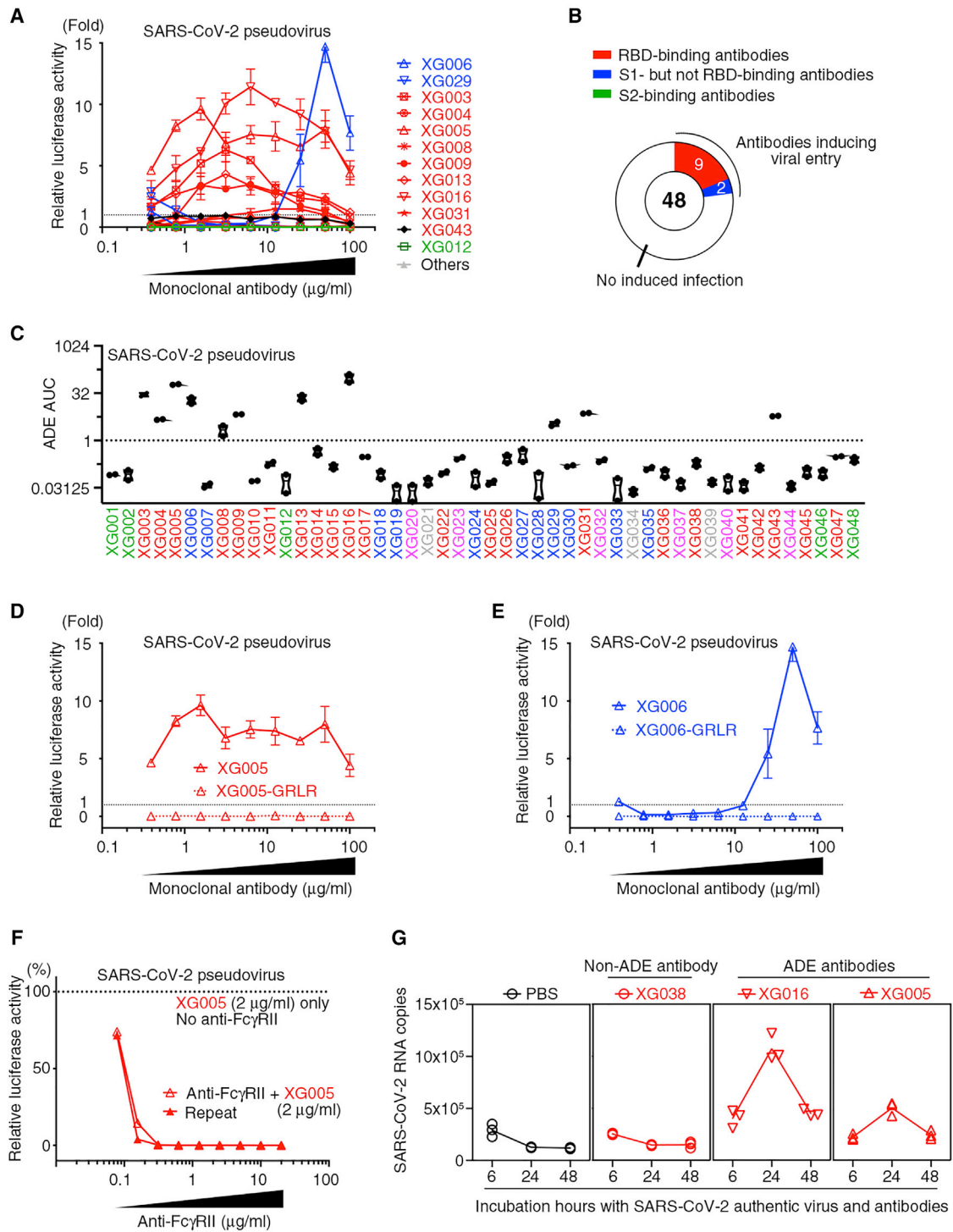


Figure 6. *In vitro* antibody-dependent viral entry by monoclonals

(A and B) *In vitro* Raji cell-dependent assays using luciferase-expressing SARS-CoV-2 pseudovirus in the presence of different dilutions of antibodies. Antibodies, which induced high levels of luciferase signal, are shown (A), including nine RBD-binding antibodies and two antibodies with S1 but no RBD binding (B). The luciferase signal induced by 2 $\mu\text{g/ml}$ of antibody XG043 (the black line) was used as a reference for normalization (100% relative luciferase activity; see the dotted lines), and others were expressed as the fold change (mean \pm range for duplicates) in luciferase activity.

(C) The corresponding AUC value for each monoclonal antibody was calculated. At least two independent experiments were performed. The signals above the dashed line were considered to represent ADE.

(legend continued on next page)

but low levels of antibody-induced viral infection, whereas antibodies from cluster Z were non-neutralizing and did not induce viral entry (Figure 7A). Further comparison using ADE AUC and neutralizing IC₅₀ verified that cluster X antibodies induced more robust antibody-dependent viral entry in Raji cells (Figure 7B), and that the antibodies from clusters X and Y (Figure 7C) and from expanded clones (Figure S7A) were more potent neutralizers.

To determine any association between antibody properties and their antigen epitopes recognized, we labeled their epitopes on the constructed tree. In cluster X, eight of nine (89%) antibodies interacted with RBD, and all of these eight antibodies, including XG009 and XG043, recognized the RBD group IV epitope (Figure 7A). This percentage was significantly higher than that in other clusters ($p = 0.001$ versus cluster Y; $p < 0.001$ versus cluster Z) (Figures 7A and 7D). Except for one group IV antibody in cluster Y, XG014, all other group IV antibodies were branched in cluster X (Figures 7A and 7D) and induced a statistically significant level of antibody-dependent viral entry in Raji cells (Figure 7E). Unsupervised hierarchical clustering was further performed using only ADE values, which alone were sufficient to produce an antibody cluster significantly associated with the RBD group IV epitopes (Figure S7B). Thus, we revealed a significant association between one of the five RBD epitopes, group IV, and ADE effects detected *in vitro*.

We also noticed that some RBD epitopes were associated with only neutralizing activity, but no ADE effect. Antibodies in cluster Y possessed neutralizing activity, but induced no or low levels of viral entry in Raji cells (Figures 7A–7C). These antibodies were directed against many distinct epitopes, including RBD group II and RBD group III epitopes. These antibodies, which recognize only group II or only group III epitopes, were not found in other clusters but just cluster Y (Figures 7A and 7D), suggesting that antibodies against these epitopes are tightly associated with neutralizing activity and induce no enhancing effects.

Therefore, we conclude that antibodies targeting two RBD epitopes (groups II and III) neutralize SARS-CoV-2 virus without enhancing activities, whereas RBD group IV antibodies are tightly associated with enhancement of SARS-CoV-2 infection *in vitro*.

DISCUSSION

Convalescent plasma shows potential benefits for treating SARS-CoV-2 infection (Duan et al., 2020; Shen et al., 2020), and many research teams used a single-cell-based antibody cloning strategy to identify monoclonal antibodies against SARS-CoV-2 for potential passive antibody administration as a

prevention and treatment. The same strategy was previously successfully used to identify potent broadly neutralizing antibodies against HIV, ZIKV, HBV, and other pathogens (Robbiani et al., 2017; Walker and Burton, 2018; Wang et al., 2020b). In the present study, we focused exclusively on one convalescent donor with potent IgG neutralization capacity, cloned and characterized his monoclonal antibodies, and investigated antibody enhancing versus neutralizing effects and their relationship with antigen epitopes.

Serological neutralizing activity against SARS-CoV-2 varied greatly among recovered individuals (Robbiani et al., 2020; Wu et al., 2020a). Unexpectedly, our result showed that the individuals with a robust serum neutralizing effect did not necessarily have potent neutralizing activity of their purified IgG antibodies (Figures 1F and 1H). This discrepancy is probably due to the neutralizing effect by non-IgG antibodies, especially by secretory IgA antibody, which plays a significant role in safeguarding mucosal surfaces against respiratory viruses. In COVID-19 patients, an early and robust serum IgA responses was observed (Cervia et al., 2020; Padoan et al., 2020; Yu et al., 2020), and monoclonal IgA antibodies have been tested as effective as IgG by *in vitro* binding and neutralizing assays (Ejemel et al., 2020; Wang et al., 2020c).

Although the ADE effect for coronaviruses has been reported *in vitro*, a potential pathological relevance during SARS-CoV-2 infection seems unlikely (Arvin et al., 2020). Clinical severity of SARS-CoV-2 infection is tightly associated with elders with pre-existing conditions, but not individuals with previous coronavirus infection (Halstead and Katzelnick, 2020). Although several monoclonals isolated from convalescent donors exhibited an enhancement of viral entry (Figure 6A), our ADE assays using sera from the exact same convalescent donors showed no ADE of SARS-CoV-2 viral entry (Figure S6A), suggesting that the concentration of ADE monoclonals is not sufficiently high among the polyclonal serum. Furthermore, our ADE assay using authentic SARS-CoV-2 virus showed an abortive replication, a phenomenon reminiscent of SARS-CoV-1 (Jaume et al., 2011). All these data imply the unlikelihood of ADE of infection/disease during SARS-CoV-2 infection. However, there is one exception, feline infectious peritonitis virus (FIPV), which causes ADE of disease in cat (Weiss and Scott, 1981). This discrepancy with SARS-CoV-1, SARS-CoV-2, and MERS-CoV could be explained by the fact that the dominant target of FIPV *in vivo* is peritoneal macrophages, but not pulmonary epithelium.

Our study revealed that 11 of 48 (23%) monoclonal anti-SARS-CoV-2 IgG antibodies displayed ADE of viral entry *in vitro*. Although this effect was Fc γ RII dependent in Raji cells, ADE of viral entry was not observed in a human erythroleukemic cell line, K562, which is also Fc γ RII positive (Zang et al., 2020),

(D and E) *In vitro* Raji cell-dependent assays using the GRLR version of XG005 (D) and XG006 (E) antibodies. Wild-type human antibody and its Fc γ receptor variants GRLR were performed in parallel on the same plate, and experiments were repeated at least two times.

(F) *In vitro* Raji cell-dependent assays with Fc γ receptor blocking. Negative control was performed without incubation of anti-human Fc γ RII antibodies with Raji cells. Experiments were repeated two times.

(G) Quantitative reverse transcription PCR results for *in vitro* Raji cell-dependent assays using authentic SARS-CoV-2 virus. The Raji cells were incubated with authentic SARS-CoV-2 virus and 4 μ g/mL non-ADE antibody XG038 or ADE antibodies XG016 or XG005, respectively. PBS was used as a negative control. At the indicated hours of incubation, cells were collected for RNA extraction and quantitative reverse transcription PCR analysis.

See also Figure S6.

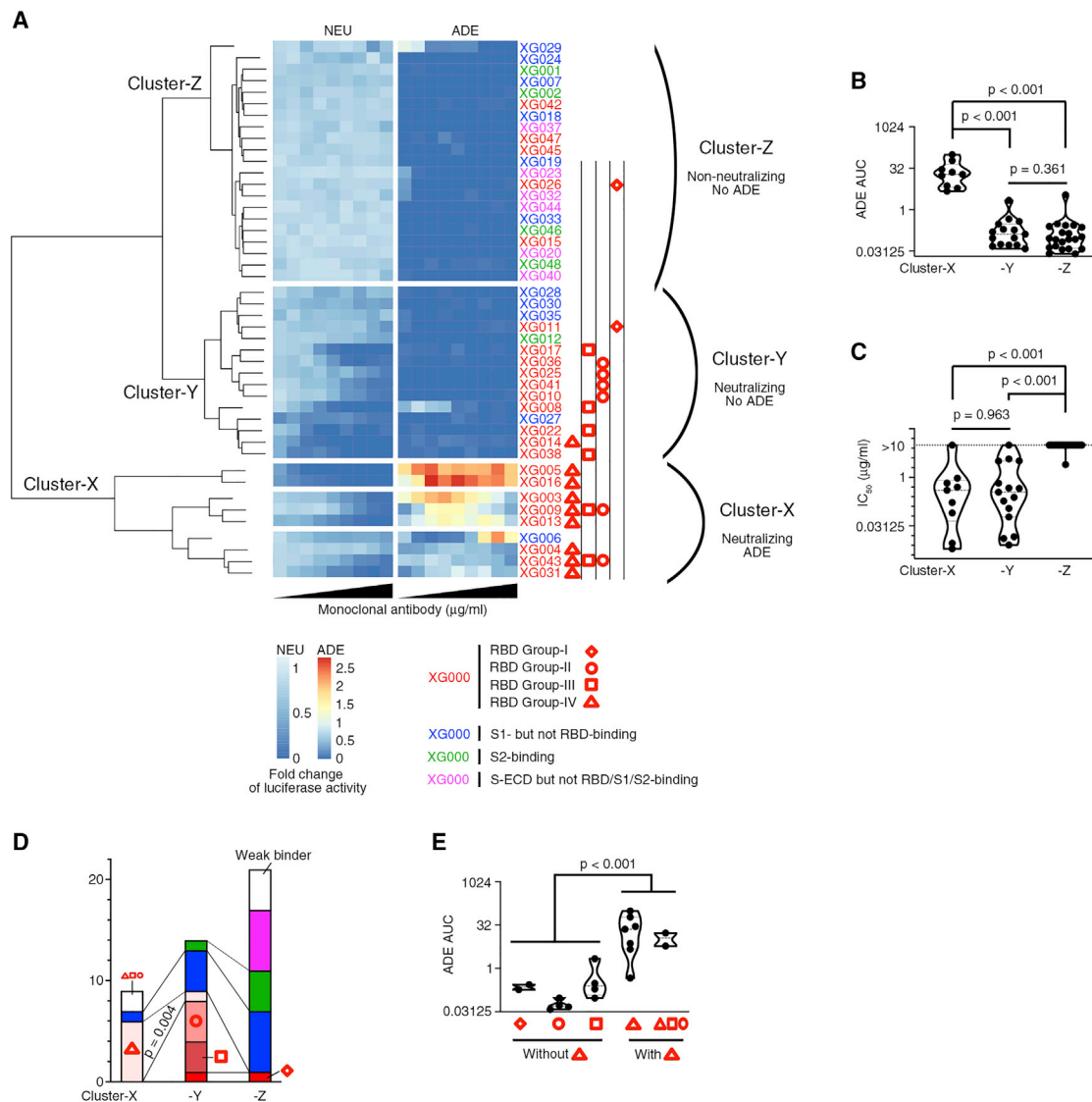


Figure 7. Clustering analysis identifies RBD epitopes associated with antibody neutralizing or enhancing effects

(A) Unsupervised hierarchical clustering was performed using the SARS-CoV-2 pseudovirus neutralization (NEU) and Raji cell-dependent (ADE) data. Clusters X, Y, and Z were identified. Antibodies with different epitopes on the S protein or RBD are color and/or shape coded, whereas antibodies with no ELISA binding against our tested antigens (XG021, XG034, XG039) were excluded. This clustering analysis was repeated using the other sets of neutralization and ADE values. (B and C) Violin plots of the ADE AUC (B) or IC_{50} values (C) of antibodies in the three clusters. In order to determine whether there is a statistically significant difference of the ADE AUC and IC_{50} values of cluster X, Y, and Z antibodies, we performed the nonparametric Dunn's Kruskal-Wallis multiple comparison test. (D) Bar graph with the number of antibodies with different binding epitopes in the three clusters. Refer to the labeling guidance of antibody epitopes in (A). Statistical analysis was performed using Fisher's exact test.

(E) Violin plots of the ADE AUC values of RBD-binding antibodies with different epitope groups. Five groups of antibodies (groups I–IV and antibody group of XG009 and XG043; see Figure 3F) were classified as two major types. One type (with Δ) contains RBD group IV antibodies or antibodies sharing group IV epitope (XG009 and XG043), while the other type (without Δ) contains group I–III antibodies, which bind non-competitively with group IV antibodies. Statistical analysis was performed using the Wilcoxon rank-sum test. See also Figure S7.

suggesting that $\text{Fc}\gamma\text{RII}$ expression is required, but not sufficient, for the antibody-dependent viral entry. Besides Raji cells, an ADE of viral entry was also demonstrated in another human Burkitt's lymphoma B cell line, Daudi, for SARS-CoV-1 (Jaume et al., 2011). Thus, it seems that B cells are more likely to be susceptible for invasion by SARS-CoV.

Uptake of viral particles through the ADE pathway might lead to the elevated production of proinflammatory cytokines (Liu et al., 2019). During SARS-CoV-2 infection, substantially elevated IgG antibody responses (Cao, 2020; Zhang et al., 2020; Zhao et al., 2020) and dramatically increased serum levels of proinflammatory cytokines (Huang et al., 2020; Wang et al.,

2020a) have been consistently observed in critically ill patients. Patients with severe COVID-19 exhibit elevated levels of proinflammatory cytokines, such as interleukin (IL)-6, IL-1 β , and IL-2. Thus, whether ADE of viral entry would lead to high levels of cytokines in B lymphocytes is another question that needs to be addressed using authentic SARS-CoV-2 virus *in vitro* and *in vivo*.

Antibodies from our donor bound to five non-overlapping RBD epitopes, similar to other studies reporting three or four distinct antigenic sites within RBD (Liu et al., 2020a; Robbani et al., 2020; Rogers et al., 2020; Wec et al., 2020; Wu et al., 2020c; Zost et al., 2020a). Importantly, we found a significant association of ADE with one of five non-overlapping antibody binding RBD epitopes. This was a surprising result given that no such epitope-ADE relationship has ever been reported for coronaviruses to the best of our knowledge. The underlying mechanism warrants further investigation.

Because SARS-CoV-1 and SARS-CoV-2 share the same human receptor, ACE2, it is possible that antibodies that are cross-reactive to these two different viruses are occasionally generated. A recent study showed that H014, a phage antibody isolated from RBD-immunized mice, showed IC₅₀ of 150 and 450 ng/ml: for SARS-CoV-1 and -2, respectively (Lv et al., 2020). Also, antibodies isolated from individuals with SARS-CoV-1 infection have been shown to be cross-neutralizing for SARS-CoV-2: antibodies ADI-55688 (IC₅₀ of 4 and >100 ng/ml for SARS-CoV-1 and -2, respectively), ADI-56046 (IC₅₀ of 20 and 50 ng/mL for SARS-CoV-1 and -2, respectively) (Wec et al., 2020), and S309 (IC₅₀ of 120 and 79 ng/mL for SARS-CoV-1 and -2, respectively) (Pinto et al., 2020). However, whether such cross-neutralizing antibodies also develop after SARS-CoV-2 infection is less established. We here identified a potent neutralizing antibody, XG014, that inhibited infection by both SARS-CoV-2 and SARS-CoV-1 with IC₅₀ values of 5.1 and 23.7 ng/mL, respectively. Therefore, XG014 is among the most potent cross-neutralizing antibodies described so far.

Importantly, XG014 did not display ADE. This was a surprising finding given that it targets the group IV RBD epitope strongly associated with ADE (Figure 7A). One possible explanation is that, after viral uptake in the form of immune complexes, the XG014 antibody binding is stable enough at acidic pH within endosomes to prevent endosomal fusion, whereas other group IV antibodies could not withstand the low pH environment. A similar hypothesis has been made for antibodies against flaviviruses (Rey et al., 2018). Another possible explanation is that the epitope recognized by XG014 is slightly different from other group IV antibodies. Further structural analysis of XG014, compared with those of other group IV ADE antibodies, would help us to decipher the correlation between ADE and epitopes in depth.

STAR★METHODS

Detailed methods are provided in the online version of this paper and include the following:

- KEY RESOURCES TABLE
- RESOURCE AVAILABILITY
 - Lead contact

- Materials availability
- Data and code availability
- EXPERIMENTAL MODEL AND SUBJECT DETAILS
 - Human subjects
 - Cell lines
 - Viruses
 - Bacteria
- METHOD DETAILS
 - Collection of human samples
 - Antibodies
 - ELISA
 - Competition ELISA
 - Preparation of SARS-CoV-2 and SARS-CoV-1 pseudotyped virus
 - *In vitro* neutralization assay by pseudotyped SARS-CoV-1 and -2 viruses
 - *In vitro* neutralization assay by authentic SARS-CoV-2 virus
 - *In vitro* assay to detect antibody-dependent viral entry
 - Protein production
 - Single cell sorting of RBD- or S-ECD-binding memory B cells
 - Antibody cloning, sequencing and production
 - Clustering analysis
- QUANTIFICATION AND STATISTICAL ANALYSIS

SUPPLEMENTAL INFORMATION

Supplemental Information can be found online at <https://doi.org/10.1016/j.celrep.2021.108699>.

ACKNOWLEDGMENTS

We would like to thank all the volunteers in this study, especially donor 16, for devoting time to our research. We thank members of the Core Facility of Microbiology and Parasitology (SHMC) of Fudan University, especially Shuhui Sun and Qian Wang, and members of Biosafety Level 3 Laboratory at Shanghai Medical College of the Fudan University for continuous support. We also thank Dr. Xiaofei Kong, Dr. Yixiao Zhang, Dr. Xiaofei Yu, and Dr. Yue Zhao for valuable suggestions and helpful discussions. This work was supported by National Natural Science Foundation of China (31872730 and 32070947 to Qiao Wang, 81822045 to L.L., and 82041025 to S.J.). This work was also supported by COVID-19 Prevention and Control Technology Project of Zhoushan, Zhejiang Province (2020C31001 to S.L. and 2020C31002 to Qiujiang Wang) and Municipal Science and Technology Plan Project of Zhoushan, Zhejiang Province (2016C11001 to S.L.). The content is solely the responsibility of the authors and does not necessarily represent the official views of any of the funding agencies or individuals.

AUTHOR CONTRIBUTIONS

Y.Z. and Zehong Liu conducted the experiments, supervised and designed the experiments, interpreted experimental results, and edited the paper. S.L. and Qiujiang Wang coordinated cohort studies and blood collection and edited the manuscript. W.X., Q.Z., C.L., Y. Wu, Y.G., C.G., X.C., and J.W. conducted experiments. Q.J. and Zhenmi Liu performed statistical analysis. I.T.S. performed computational analysis. C.T.M., S.J., D.Q., X.W., and T.Y. discussed experiments, interpreted experimental results, and edited the manuscript. Y.X., Z.Y., and Y. Wen supervised and designed experiments in Biosafety Level 3 Laboratory and edited the manuscript. L.L. and Qiao Wang conceived the study; supervised, designed, and interpreted experiments; and wrote the paper.

DECLARATION OF INTERESTS

Qiao Wang, L.L., Y.Z., and Zezhong Liu have a provisional patent application. The other authors declare no competing interests.

Received: August 19, 2020
Revised: October 27, 2020
Accepted: January 6, 2021
Published: January 12, 2021

REFERENCES

- Andreato, E., Nicastrì, E., Paciello, I., Pileri, P., Manganaro, N., Piccini, G., Manenti, A., Pantano, E., Kabanova, A., Troisi, M., et al. (2020). Identification of neutralizing human monoclonal antibodies from Italian Covid-19 convalescent patients. *bioRxiv*. <https://doi.org/10.1101/2020.05.05.078154>.
- Arvin, A.M., Fink, K., Schmid, M.A., Cathcart, A., Spreafico, R., Havenar-Daughton, C., Lanzavecchia, A., Corti, D., and Virgin, H.W. (2020). A perspective on potential antibody-dependent enhancement of SARS-CoV-2. *Nature* 584, 353–363.
- Bardina, S.V., Bunduc, P., Tripathi, S., Duehr, J., Frere, J.J., Brown, J.A., Nachbagauer, R., Foster, G.A., Krzyzstof, D., Tortorella, D., et al. (2017). Enhancement of Zika virus pathogenesis by preexisting antinflavivirus immunity. *Science* 356, 175–180.
- Brochet, X., Lefranc, M.P., and Giudicelli, V. (2008). IMGT/V-QUEST: the highly customized and integrated system for IG and TR standardized V-J and V-D-J sequence analysis. *Nucleic Acids Res.* 36 (*Web Server issue*), W503–W508.
- Brouwer, P.J.M., Daniels, T.G., van der Straten, K., Snitselaar, J.L., Aldon, Y., Bangaru, S., Torres, J.L., Okba, N.M.A., Claireaux, M., Kerster, G., et al. (2020). Potent neutralizing antibodies from COVID-19 patients define multiple targets of vulnerability. *Science* 369, 643–650.
- Cao, X. (2020). COVID-19: immunopathology and its implications for therapy. *Nat. Rev. Immunol.* 20, 269–270.
- Cao, Y., Su, B., Guo, X., Sun, W., Deng, Y., Bao, L., Zhu, Q., Zhang, X., Zheng, Y., Geng, C., et al. (2020). Potent neutralizing antibodies against SARS-CoV-2 identified by high-throughput single-cell sequencing of convalescent patients' B cells. *Cell* 182, 73–84.e16.
- Cervia, C., Nilsson, J., Zurbuchen, Y., Valaperti, A., Schreiner, J., Wolfensberger, A., Raeber, M.E., Adamo, S., Emmenegger, M., Hasler, S., et al. (2020). Systemic and mucosal antibody secretion specific to SARS-CoV-2 during mild versus severe COVID-19. *bioRxiv*. <https://doi.org/10.1101/2020.05.21.108308>.
- Chen, X., Li, R., Pan, Z., Qian, C., Yang, Y., You, R., Zhao, J., Liu, P., Gao, L., Li, Z., et al. (2020). Human monoclonal antibodies block the binding of SARS-CoV-2 spike protein to angiotensin converting enzyme 2 receptor. *Cell. Mol. Immunol.* 17, 647–649.
- Chi, X., Yan, R., Zhang, J., Zhang, G., Zhang, Y., Hao, M., Zhang, Z., Fan, P., Dong, Y., Yang, Y., et al. (2020). A neutralizing human antibody binds to the N-terminal domain of the Spike protein of SARS-CoV-2. *Science* 369, 650–655.
- Coronaviridae Study Group of the International Committee on Taxonomy of Viruses (2020). The species Severe acute respiratory syndrome-related coronavirus: classifying 2019-nCoV and naming it SARS-CoV-2. *Nat. Microbiol.* 5, 536–544.
- Duan, K., Liu, B., Li, C., Zhang, H., Yu, T., Qu, J., Zhou, M., Chen, L., Meng, S., Hu, Y., et al. (2020). Effectiveness of convalescent plasma therapy in severe COVID-19 patients. *Proc. Natl. Acad. Sci. USA* 117, 9490–9496.
- Ejemel, M., Li, Q., Hou, S., Schiller, Z.A., Wallace, A.L., Amcheslavsky, A., Yilmaz, N.K., Toomey, J.R., Schneider, R., Close, B.J., et al. (2020). IgA MAb blocks SARS-CoV-2 Spike-ACE2 interaction providing mucosal immunity. *bioRxiv*. <https://doi.org/10.1101/2020.05.15.096719>.
- Eroshenko, N., Gill, T., Keaveney, M.K., Church, G.M., Trevejo, J.M., and Rajaniemi, H. (2020). Implications of antibody-dependent enhancement of infection for SARS-CoV-2 countermeasures. *Nat. Biotechnol.* 38, 789–791.
- Escolano, A., Gristick, H.B., Abernathy, M.E., Merckenschlager, J., Gautam, R., Oliveira, T.Y., Pai, J., West, A.P., Jr., Barnes, C.O., Cohen, A.A., et al. (2019). Immunization expands B cells specific to HIV-1 V3 glycan in mice and macaques. *Nature* 570, 468–473.
- Gu, C., Wu, Y., Guo, H., Zhu, Y., Xu, W., Wang, Y., Sun, Z., Cai, X., Li, Y., Liu, J., et al. (2020). Potent antiviral effect of protoporphyrin IX and verteporfin on SARS-CoV-2 infection. *bioRxiv*. <https://doi.org/10.1101/2020.04.30.071290>.
- Halstead, S.B., and Katzelnick, L. (2020). COVID-19 Vaccines: Should we fear ADE? *J. Infect. Dis.* 222, 1946–1950.
- Hansen, J., Baum, A., Pascal, K.E., Russo, V., Giordano, S., Wloga, E., Fulton, B.O., Yan, Y., Koon, K., Patel, K., et al. (2020). Studies in humanized mice and convalescent humans yield a SARS-CoV-2 antibody cocktail. *Science* 369, 1010–1014.
- Horton, H.M., Bernett, M.J., Pong, E., Peipp, M., Karki, S., Chu, S.Y., Richards, J.O., Vostiar, I., Joyce, P.F., Repp, R., et al. (2008). Potent in vitro and in vivo activity of an Fc-engineered anti-CD19 monoclonal antibody against lymphoma and leukemia. *Cancer Res.* 68, 8049–8057.
- Huang, C., Wang, Y., Li, X., Ren, L., Zhao, J., Hu, Y., Zhang, L., Fan, G., Xu, J., Gu, X., et al. (2020). Clinical features of patients infected with 2019 novel coronavirus in Wuhan, China. *Lancet* 395, 497–506.
- Iwasaki, A., and Yang, Y. (2020). The potential danger of suboptimal antibody responses in COVID-19. *Nat. Rev. Immunol.* 20, 339–341.
- Jaume, M., Yip, M.S., Cheung, C.Y., Leung, H.L., Li, P.H., Kien, F., Dutry, I., Callendret, B., Escriou, N., Altmeyer, R., et al. (2011). Anti-severe acute respiratory syndrome coronavirus spike antibodies trigger infection of human immune cells via a pH- and cysteine protease-independent FcγR pathway. *J. Virol.* 85, 10582–10597.
- Jiang, S., Du, L., and Shi, Z. (2020a). An emerging coronavirus causing pneumonia outbreak in Wuhan, China: calling for developing therapeutic and prophylactic strategies. *Emerg. Microbes Infect.* 9, 275–277.
- Jiang, S., Hillyer, C., and Du, L. (2020b). Neutralizing Antibodies against SARS-CoV-2 and Other Human Coronaviruses. *Trends Immunol.* 41, 355–359.
- Jiang, S., Shi, Z., Shu, Y., Song, J., Gao, G.F., Tan, W., and Guo, D. (2020c). A distinct name is needed for the new coronavirus. *Lancet* 395, 949.
- Ju, B., Zhang, Q., Ge, J., Wang, R., Sun, J., Ge, X., Yu, J., Shan, S., Zhou, B., Song, S., et al. (2020). Human neutralizing antibodies elicited by SARS-CoV-2 infection. *Nature* 584, 115–119.
- Katzelnick, L.C., Gresh, L., Halloran, M.E., Mercado, J.C., Kuan, G., Gordon, A., Balmaseda, A., and Harris, E. (2017). Antibody-dependent enhancement of severe dengue disease in humans. *Science* 358, 929–932.
- Korber, B., Fischer, W.M., Gnanakaran, S., Yoon, H., Theiler, J., Abfalterer, W., Hengartner, N., Giorgi, E.E., Bhattacharya, T., Foley, B., et al.; Sheffield COVID-19 Genomics Group (2020). Tracking Changes in SARS-CoV-2 Spike: Evidence that D614G Increases Infectivity of the COVID-19 Virus. *Cell* 182, 812–827.e19.
- Kreer, C., Zehner, M., Weber, T., Ercanoglu, M.S., Gieselmann, L., Rohde, C., Halwe, S., Korenkov, M., Schommers, P., Vanshylla, K., et al. (2020). Longitudinal Isolation of Potent Near-Germline SARS-CoV-2-Neutralizing Antibodies from COVID-19 Patients. *Cell* 182, 843–854.e12.
- Li, F. (2016). Structure, Function, and Evolution of Coronavirus Spike Proteins. *Annu. Rev. Virol.* 3, 237–261.
- Li, Q., Wu, J., Nie, J., Zhang, L., Hao, H., Liu, S., Zhao, C., Zhang, Q., Liu, H., Nie, L., et al. (2020). The Impact of Mutations in SARS-CoV-2 Spike on Viral Infectivity and Antigenicity. *Cell* 182, 1284–1294.e9.
- Liu, L., Wei, Q., Lin, Q., Fang, J., Wang, H., Kwok, H., Tang, H., Nishiura, K., Peng, J., Tan, Z., et al. (2019). Anti-spike IgG causes severe acute lung injury by skewing macrophage responses during acute SARS-CoV infection. *JCI Insight* 4, 123158.
- Liu, L., Wang, P., Nair, M.S., Yu, J., Rapp, M., Wang, Q., Luo, Y., Chan, J.F., Sahi, V., Figueroa, A., et al. (2020a). Potent neutralizing monoclonal antibodies directed to multiple epitopes on the SARS-CoV-2 spike. <https://doi.org/10.1101/2020.06.17.153486>.

Liu, X., Gao, F., Gou, L., Chen, Y., Gu, Y., Ao, L., Shen, H., Hu, Z., Guo, X., and Gao, W. (2020b). Neutralizing Antibodies Isolated by a site-directed Screening have Potent Protection on SARS-CoV-2 Infection. *bioRxiv*. <https://doi.org/10.1101/2020.05.03.074914>.

Lv, Z., Deng, Y.Q., Ye, Q., Cao, L., Sun, C.Y., Fan, C., Huang, W., Sun, S., Sun, Y., Zhu, L., et al. (2020). Structural basis for neutralization of SARS-CoV-2 and SARS-CoV by a potent therapeutic antibody. *Science* 369, 1505–1509.

Miner, J.J., and Diamond, M.S. (2017). Dengue Antibodies, then Zika: A Fatal Sequence in Mice. *Immunity* 46, 771–773.

Ou, J., Zhou, Z., Dai, R., Zhang, J., Lan, W., Zhao, S., Wu, J., Seto, D., Cui, L., Zhang, G., et al. (2020). Emergence of RBD mutations in circulating SARS-CoV-2 strains enhancing the structural stability and human ACE2 receptor affinity of the spike protein. *bioRxiv*. <https://doi.org/10.1101/2020.03.15.991844>.

Padoan, A., Sciacovelli, L., Basso, D., Negrini, D., Zuin, S., Cosma, C., Fagjan, D., Matricardi, P., and Plebani, M. (2020). IgA-Ab response to spike glycoprotein of SARS-CoV-2 in patients with COVID-19: A longitudinal study. *Clin. Chim. Acta* 507, 164–166.

Pinto, D., Park, Y.J., Beltramello, M., Walls, A.C., Tortorici, M.A., Bianchi, S., Jaconi, S., Culap, K., Zatta, F., De Marco, A., et al. (2020). Cross-neutralization of SARS-CoV-2 by a human monoclonal SARS-CoV antibody. *Nature* 583, 290–295.

Premkumar, L., Segovia-Chumbez, B., Jadi, R., Martinez, D.R., Raut, R., Markmann, A., Cornaby, C., Bartelt, L., Weiss, S., Park, Y., et al. (2020). The receptor binding domain of the viral spike protein is an immunodominant and highly specific target of antibodies in SARS-CoV-2 patients. *Sci. Immunol.* 5, eabc8413.

Rey, F.A., Stiasny, K., Vaney, M.C., Dellarole, M., and Heinz, F.X. (2018). The bright and the dark side of human antibody responses to flaviviruses: lessons for vaccine design. *EMBO Rep.* 19, 206–224.

Robbiani, D.F., Bozzacco, L., Keeffe, J.R., Khouri, R., Olsen, P.C., Gazumyan, A., Schaefer-Babajew, D., Avila-Rios, S., Nogueira, L., Patel, R., et al. (2017). Recurrent Potent Human Neutralizing Antibodies to Zika Virus in Brazil and Mexico. *Cell* 169, 597–609.e11.

Robbiani, D.F., Olsen, P.C., Costa, F., Wang, Q., Oliveira, T.Y., Nery, N., Jr., Aromolaran, A., do Rosário, M.S., Sacramento, G.A., Cruz, J.S., et al. (2019). Risk of Zika microcephaly correlates with features of maternal antibodies. *J. Exp. Med.* 216, 2302–2315.

Robbiani, D.F., Gaebler, C., Muecksch, F., Lorenzi, J.C.C., Wang, Z., Cho, A., Agudelo, M., Barnes, C.O., Gazumyan, A., Finkin, S., et al. (2020). Convergent antibody responses to SARS-CoV-2 in convalescent individuals. *Nature* 584, 437–442.

Rogers, T.F., Zhao, F., Huang, D., Beutler, N., Burns, A., He, W.T., Limbo, O., Smith, C., Song, G., Woehl, J., et al. (2020). Isolation of potent SARS-CoV-2 neutralizing antibodies and protection from disease in a small animal model. *Science* 369, 956–963.

Salje, H., Cummings, D.A.T., Rodriguez-Barraquer, I., Katzelnick, L.C., Lessler, J., Klungthong, C., Thaisomboonsuk, B., Nisalak, A., Weg, A., Ellison, D., et al. (2018). Reconstruction of antibody dynamics and infection histories to evaluate dengue risk. *Nature* 557, 719–723.

Scheid, J.F., Mouquet, H., Feldhahn, N., Walker, B.D., Pereyra, F., Cutrell, E., Seaman, M.S., Mascola, J.R., Wyatt, R.T., Wardemann, H., and Nussenzweig, M.C. (2009). A method for identification of HIV gp140 binding memory B cells in human blood. *J. Immunol. Methods* 343, 65–67.

Seydoux, E., Homad, L.J., MacCamy, A.J., Parks, K.R., Hurlburt, N.K., Jennewein, M.F., Akins, N.R., Stuart, A.B., Wan, Y.H., Feng, J., et al. (2020). Analysis of a SARS-CoV-2-Infected Individual Reveals Development of Potent Neutralizing Antibodies with Limited Somatic Mutation. *Immunity* 53, 98–105.e5.

Shen, C., Wang, Z., Zhao, F., Yang, Y., Li, J., Yuan, J., Wang, F., Li, D., Yang, M., Xing, L., et al. (2020). Treatment of 5 Critically Ill Patients With COVID-19 With Convalescent Plasma. *JAMA* 323, 1582–1589.

Sui, J., Aird, D.R., Tamin, A., Murakami, A., Yan, M., Yammanuru, A., Jing, H., Kan, B., Liu, X., Zhu, Q., et al. (2008). Broadening of neutralization activity to

directly block a dominant antibody-driven SARS-coronavirus evolution pathway. *PLoS Pathog.* 4, e1000197.

Sun, Z., Chen, C., Li, W., Martinez, D.R., Drelich, A., Baek, D.S., Liu, X., Melors, J.W., Tseng, C.T., Baric, R.S., and Dimitrov, D.S. (2020). Potent neutralization of SARS-CoV-2 by human antibody heavy-chain variable domains isolated from a large library with a new stable scaffold. *MAbs* 12, 1778435.

Tang, X.C., Agnihothram, S.S., Jiao, Y., Stanhope, J., Graham, R.L., Peterson, E.C., Avnir, Y., Tallarico, A.S., Sheehan, J., Zhu, Q., et al. (2014). Identification of human neutralizing antibodies against MERS-CoV and their role in virus adaptive evolution. *Proc. Natl. Acad. Sci. USA* 111, E2018–E2026.

ter Meulen, J., van den Brink, E.N., Poon, L.L., Marissen, W.E., Leung, C.S., Cox, F., Cheung, C.Y., Bakker, A.Q., Bogaards, J.A., van Deventer, E., et al. (2006). Human monoclonal antibody combination against SARS coronavirus: synergy and coverage of escape mutants. *PLoS Med.* 3, e237.

Tian, X., Li, C., Huang, A., Xia, S., Lu, S., Shi, Z., Lu, L., Jiang, S., Yang, Z., Wu, Y., and Ying, T. (2020). Potent binding of 2019 novel coronavirus spike protein by a SARS coronavirus-specific human monoclonal antibody. *Emerg. Microbes Infect.* 9, 382–385.

von Boehmer, L., Liu, C., Ackerman, S., Gitlin, A.D., Wang, Q., Gazumyan, A., and Nussenzweig, M.C. (2016). Sequencing and cloning of antigen-specific antibodies from mouse memory B cells. *Nat. Protoc.* 11, 1908–1923.

Walker, L.M., and Burton, D.R. (2018). Passive immunotherapy of viral infections: ‘super-antibodies’ enter the fray. *Nat. Rev. Immunol.* 18, 297–308.

Wan, J., Xing, S., Ding, L., Wang, Y., Gu, C., Wu, Y., Rong, B., Li, C., Wang, S., Chen, K., et al. (2020). Human-IgG-Neutralizing Monoclonal Antibodies Block the SARS-CoV-2 Infection. *Cell Rep.* 32, 107918.

Wang, S.F., Tseng, S.P., Yen, C.H., Yang, J.Y., Tsao, C.H., Shen, C.W., Chen, K.H., Liu, F.T., Liu, W.T., Chen, Y.M., and Huang, J.C. (2014). Antibody-dependent SARS coronavirus infection is mediated by antibodies against spike proteins. *Biochem. Biophys. Res. Commun.* 451, 208–214.

Wang, J., Jiang, M., Chen, X., and Montaner, L.J. (2020a). Cytokine storm and leukocyte changes in mild versus severe SARS-CoV-2 infection: Review of 3939 COVID-19 patients in China and emerging pathogenesis and therapy concepts. *J. Leukoc. Biol.* 108, 17–41.

Wang, Q., Michailidis, E., Yu, Y., Wang, Z., Hurley, A.M., Oren, D.A., Mayer, C.T., Gazumyan, A., Liu, Z., Zhou, Y., et al. (2020b). A Combination of Human Broadly Neutralizing Antibodies against Hepatitis B Virus HBsAg with Distinct Epitopes Suppresses Escape Mutations. *Cell Host Microbe* 28, 335–349.e6.

Wang, Z., Lorenzi, J.C.C., Muecksch, F., Finkin, S., Viant, C., Gaebler, C., Ci-polla, M., Hoffman, H.H., Oliveira, T.Y., Oren, D.A., et al. (2020c). Enhanced SARS-CoV-2 Neutralization by Secretory IgA in vitro. *bioRxiv*. <https://doi.org/10.1101/2020.09.09.288555>.

Wec, A.Z., Wrapp, D., Herbert, A.S., Maurer, D.P., Haslwanter, D., Sakharkar, M., Jangra, R.K., Dieterle, M.E., Lilov, A., Huang, D., et al. (2020). Broad neutralization of SARS-related viruses by human monoclonal antibodies. *Science* 369, 731–736.

Weiss, R.C., and Scott, F.W. (1981). Pathogenesis of feline infectious peritonitis: nature and development of viremia. *Am. J. Vet. Res.* 42, 382–390.

Wu, F., Wang, A., Liu, M., Wang, Q., Chen, J., Xia, S., Ling, Y., Zhang, Y., Xun, J., Lu, L., et al. (2020a). Neutralizing antibody responses to SARS-CoV-2 in a COVID-19 recovered patient cohort and their implications. *bioRxiv*. <https://doi.org/10.1101/2020.03.30.20047365>.

Wu, Y., Li, C., Xia, S., Tian, X., Kong, Y., Wang, Z., Gu, C., Zhang, R., Tu, C., Xie, Y., et al. (2020b). Identification of Human Single-Domain Antibodies against SARS-CoV-2. *Cell Host Microbe* 27, 891–898.e5.

Wu, Y., Wang, F., Shen, C., Peng, W., Li, D., Zhao, C., Li, Z., Li, S., Bi, Y., Yang, Y., et al. (2020c). A noncompeting pair of human neutralizing antibodies block COVID-19 virus binding to its receptor ACE2. *Science* 368, 1274–1278.

Xia, S., Liu, M., Wang, C., Xu, W., Lan, Q., Feng, S., Qi, F., Bao, L., Du, L., Liu, S., et al. (2020a). Inhibition of SARS-CoV-2 (previously 2019-nCoV) infection by a highly potent pan-coronavirus fusion inhibitor targeting its spike protein that harbors a high capacity to mediate membrane fusion. *Cell Res.* 30, 343–355.

- Xia, S., Zhu, Y., Liu, M., Lan, Q., Xu, W., Wu, Y., Ying, T., Liu, S., Shi, Z., Jiang, S., and Lu, L. (2020b). Fusion mechanism of 2019-nCoV and fusion inhibitors targeting HR1 domain in spike protein. *Cell. Mol. Immunol.* *17*, 765–767.
- Ye, J., Ma, N., Madden, T.L., and Ostell, J.M. (2013). IgBLAST: an immunoglobulin variable domain sequence analysis tool. *Nucleic Acids Res.* *41* (*Web Server issue*), W34–W40.
- Yip, M.S., Leung, N.H., Cheung, C.Y., Li, P.H., Lee, H.H., Daëron, M., Peiris, J.S., Bruzzone, R., and Jaume, M. (2014). Antibody-dependent infection of human macrophages by severe acute respiratory syndrome coronavirus. *Virology* *11*, 82.
- Yu, H.Q., Sun, B.Q., Fang, Z.F., Zhao, J.C., Liu, X.Y., Li, Y.M., Sun, X.Z., Liang, H.F., Zhong, B., Huang, Z.F., et al. (2020). Distinct features of SARS-CoV-2-specific IgA response in COVID-19 patients. *Eur. Respir. J.* *56*, 2001526.
- Yuan, M., Wu, N.C., Zhu, X., Lee, C.D., So, R.T.Y., Lv, H., Mok, C.K.P., and Wilson, I.A. (2020). A highly conserved cryptic epitope in the receptor binding domains of SARS-CoV-2 and SARS-CoV. *Science* *368*, 630–633.
- Zang, J., Gu, C., Zhou, B., Zhang, C., Yang, Y., Xu, S., Zhang, X., Zhou, Y., Bai, L., Wu, Y., et al. (2020). Immunization with the receptor-binding domain of SARS-CoV-2 elicits antibodies cross-neutralizing SARS-CoV-2 and SARS-CoV without antibody-dependent enhancement. *bioRxiv*. <https://doi.org/10.1101/2020.05.21.107565>.
- Zhang, B., Zhou, X., Zhu, C., Song, Y., Feng, F., Qiu, Y., Feng, J., Jia, Q., Song, Q., Zhu, B., and Wang, J. (2020). Immune Phenotyping Based on the Neutrophil-to-Lymphocyte Ratio and IgG Level Predicts Disease Severity and Outcome for Patients With COVID-19. *Front. Mol. Biosci.* *7*, 157.
- Zhao, J., Yuan, Q., Wang, H., Liu, W., Liao, X., Su, Y., Wang, X., Yuan, J., Li, T., Li, J., et al. (2020). Antibody responses to SARS-CoV-2 in patients with novel coronavirus disease 2019. *Clin. Infect. Dis.* *71*, 2027–2034.
- Zhou, P., Yang, X.L., Wang, X.G., Hu, B., Zhang, L., Zhang, W., Si, H.R., Zhu, Y., Li, B., Huang, C.L., et al. (2020). A pneumonia outbreak associated with a new coronavirus of probable bat origin. *Nature* *579*, 270–273.
- Zhu, N., Zhang, D., Wang, W., Li, X., Yang, B., Song, J., Zhao, X., Huang, B., Shi, W., Lu, R., et al.; China Novel Coronavirus Investigating and Research Team (2020). A Novel Coronavirus from Patients with Pneumonia in China, 2019. *N. Engl. J. Med.* *382*, 727–733.
- Zost, S.J., Gilchuk, P., Case, J.B., Binshtein, E., Chen, R.E., Nkolola, J.P., Schäfer, A., Reidy, J.X., Trivette, A., Nargi, R.S., et al. (2020a). Potently neutralizing and protective human antibodies against SARS-CoV-2. *Nature* *584*, 443–449.
- Zost, S.J., Gilchuk, P., Chen, R.E., Case, J.B., Reidy, J.X., Trivette, A., Nargi, R.S., Sutton, R.E., Suryadevara, N., Chen, E.C., et al. (2020b). Rapid isolation and profiling of a diverse panel of human monoclonal antibodies targeting the SARS-CoV-2 spike protein. *Nat. Med.* *26*, 1422–1427.

STAR★METHODS

KEY RESOURCES TABLE

Reagent or resource	Source	Identifier
Antibodies		
Goat anti-Human IgG (H+L) secondary antibody, HRP	Thermo Fisher Scientific	Cat#31410; RRID: AB_228269
Mouse anti-human IgG Fab antibody (HRP)	GenScript	Cat#A01855-200
Mouse anti-human CD20-PECy7	BD PharMingen	Cat#560735; RRID: AB_399985
APC Mouse anti-human CD19	BD PharMingen	Cat#555415
Anti-CD27-PE	BD Biosciences	Cat#555441; RRID: AB_395834
Anti-hCD32	BD PharMingen	Cat#557333
Anti-HBs H004	Wang et al., 2020b	N/A
CR3022	ter Meulen et al., 2006	N/A
Anti-N polyclonal antibody	Gu et al., 2020	N/A
Bacterial and virus strains		
<i>E. Coli</i> Trans5α chemically Competent Cells	TransGen Biotech	Cat#CD201-01
Authentic SARS-CoV-2 virus, nCoV-SH01 (GenBank: MT121215.1)	Wu et al., 2020b	N/A
Chemicals, peptides, and recombinant proteins		
Streptavidin HRP	BD Biosciences	Cat#554066
Streptavidin APC	BD Biosciences	Cat#554067; RRID: AB_10050396
Streptavidin PE	eBioscience	Cat#12-4317-87
Human BD Fc Block	BD PharMingen	Cat#564220
SARS-CoV-2 S protein (RBD)	GenScript	Cat#Z03479
SARS-CoV-2 S1 protein	GenScript	Cat#Z03501
Recombinant 2019-nCoV S2 protein (C-Fc)	Novoprotein	Cat#DRA48
SARS-CoV-2 Spike protein (ECD, His & Flag tag)	GenScript	Cat#Z03481
Insect-C-His NP	GenScript	Cat#Z03480
Recombinant 2019 nCoV Spike S (amino acid 14-1212)	Kactus Biosystems	Cat#COV-VM5SS
Recombinant 2019 nCoV Spike RBD	Kactus Biosystems	Cat#COV-VM4BD
RNAasin Plus RNase inhibitor	Promega	Cat#N2615
4 × dNTPS (100 mM)	Solarbio Life Sciences	Cat#PC2300
DNase/RNase-Free water	Solarbio Life Sciences	Cat#R1600
PBS (10 ×), pH 7.2-7.4	Solarbio Life Sciences	Cat#P1022
1 M Tris-HCl, pH 9.0	Solarbio Life Sciences	Cat#T1160
IGEPAL CA-630	Sigma	Cat#18896
Dimethyl Sulfoxide	Sigma	Cat#2650
Bovine Serum Albumin	WeiAo Biotech, Shanghai	Cat#WH3044
Fetal Bovine Serum	GEMINI	Cat#900-108
UltraPure Sucrose	Macklin Biochemical	Cat#S824459
Cresol Red sodium salt	Macklin Biochemical	Cat#C806031
ABTS Chromogen / substrate solution for ELISA	Thermo Fisher Scientific	Cat#00-2024
UltraPure 0.5M EDTA, pH 8.0	Invitrogen	Cat#15575-038
Hank's Balanced Salt Mixture (D-Hanks)	Solarbio Life Sciences	Cat#H1045-500
EZ Trans	Life iLAB Bio Technology, Shanghai	Cat#AC04L082

(Continued on next page)

Continued

Reagent or resource	Source	Identifier
TRIzol LS Reagent	Thermo Fisher Scientific	Cat# 10296010
Critical commercial assays		
LS magnetic columns	Miltenyi Biotech	Cat#130-042-401
CD19 MicroBeads, human	Miltenyi Biotech	Cat#130-097-055
EZ-Link Sulfo-NHS-LC Biotin, No weight format	Thermo Fisher Scientific	Cat#39257
BirA Biotin-Protein Ligase Kit	Avidity	Cat#BIRA500
Zeba Spin Desalting Columns, 7K MWCO	Thermo Fisher Scientific	Cat#89889
Superscript III Reverse Transcriptase	Thermo Fisher Scientific	Cat#18080044
HotStarTaq DNA Polymerase	QIAGEN	Cat#203209
Protein G Sepharose 4 Fast Flow	GE Healthcare	Cat#17061805
Pierce™ IgG Elution buffer	Thermo Fisher Scientific	Cat#21004
Histopaque-10771	Sigma	Cat#10771
Agel-HF	New England BioLabs	Cat#R3552L
BsiwI-HF	New England BioLabs	Cat#R3553L
XhoI	New England BioLabs	Cat#R0146L
Sall-HF	New England BioLabs	Cat#R3138S
T4 DNA polymerase	New England BioLabs	Cat#M0203L
One Step PrimeScript RT-PCR Kit	Takara	Cat#RR064B
Luciferase Assay System	Promega	Cat#E1501
Experimental models: cell lines		
HEK293F cell line	(Wu et al., 2020b)	N/A
HEK293T cell line	(Xia et al., 2020a)	N/A
Expi293 Expression System	Thermo Fisher Scientific	Cat#A14635
Huh-7 cell line	(Xia et al., 2020a)	N/A
Vero-E6 cell line	(Xia et al., 2020a)	N/A
Raji cell line	(Jaume et al., 2011)	N/A
Oligonucleotides		
Random Primers	Thermo Fisher Scientific	Cat#48190011
Recombinant DNA		
IG γ 1 expression vector	von Boehmer et al., 2016	N/A
IG κ expression vector	von Boehmer et al., 2016	N/A
IG λ expression vector	von Boehmer et al., 2016	N/A
pNL4-3.luc.RE	Xia et al., 2020a	N/A
pcDNA3.1-SARS-CoV-1-S	Xia et al., 2020a	N/A
pcDNA3.1-SARS-COV-2-S	Xia et al., 2020a	N/A
IG γ 1-GRLR expression vector	Robbiani et al., 2019	N/A
Software and algorithms		
PRISM	GraphPad	https://www.graphpad.com
IgBlast	Ye et al., 2013	https://www.ncbi.nlm.nih.gov/igblast/
IMGT/V-QUEST	Brochet et al., 2008	http://www.imgt.org/IMGT_vquest/vquest
Others		
Sterile 50 ml Disposable Vacuum Filtration System	Millipore Sigma	Cat#SCGP00525
Amicon Ultra-4 Centrifugal Filters Ultracel-30K	Merck Millipore Ltd.	Cat#UFC803096
Ultrafree-MC Centrifugal filter units, 0.22 μ M GV DURAPORE	Merck Millipore Ltd.	Cat#UFC30GV0S
Pipet-Lite Multi Pipette L12-20XLS+	RAININ	Cat#17013808
General Long-Term Storage Cryogenic Tubes	Nalgene	Cat#5000-1020

(Continued on next page)

Continued

Reagent or resource	Source	Identifier
SimpliAmp Thermal Cycler	Thermo Fisher Scientific	Cat#A24812
500 mL Bottle Top Vacuum Filter, 0.20 μm Pore	Thermo Fisher Scientific	Cat#566-0020
ACCUSPIN Tubes Sterile, 50ml Capacity	Sigma	Cat#A2055-10EA

RESOURCE AVAILABILITY

Lead contact

Further information and requests for resources and reagents should be directed to and will be fulfilled by the Lead Contact, Qiao Wang (wangqiao@fudan.edu.cn).

Materials availability

All unique reagents generated in this study are available from the Lead Contact with a completed Materials Transfer Agreement. Sharing of antibodies with academic researchers may require a payment to cover the cost of generation and a completed Material Transfer Agreement.

Data and code availability

The published article includes all datasets generated or analyzed during this study. Original data have been deposited Mendeley data: <https://data.mendeley.com/datasets/bjpk4bzsd/1>.

EXPERIMENTAL MODEL AND SUBJECT DETAILS

Human subjects

Volunteer recruitment and blood draws were performed at the Zhoushan Hospital under a protocol approved by the Zhoushan Hospital Research Ethics Committee (2020-003). Experiments related to all human samples were performed at the School of Basic Medical Sciences, Fudan University under a protocol approved by the institutional Ethics Committee (2020-C007). Study participants, 16 convalescent donors, whose infections have been confirmed by PCR, and 8 unexposed naive donors. All donors ranged in age from 7-67 with a mean of 37, and the female:male ratio was 14:10 (Figure S1B).

Cell lines

Human embryonic kidney 293T (HEK293T) cells, human hepatoma Huh-7 cells and African green monkey kidney Vero-E6 cells (Xia et al., 2020a) were maintained in Dulbecco's Modified Eagle Medium (DMEM) supplemented with 10% heat-inactivated fetal bovine serum (FBS), 100 U/ml penicillin, and 100 mg/ml streptomycin. Raji cells (human Burkitt's lymphoma B lymphoblast) (Jaume et al., 2011), were maintained in RPMI 1640 supplemented with 10% FBS, 100 U/ml penicillin, and 100 mg/ml streptomycin. All cell lines were cultured at 37°C in 5% CO₂. Human embryonic kidney 293F (HEK293F) suspension cells were cultured using HEK293 serum-free OPM-293-CD05 medium (OPM Biosciences) at 37°C in 5% CO₂ with shaking at 100 rpm.

Viruses

The authentic SARS-CoV-2 virus, nCoV-SH01 (GenBank: MT121215.1) used in this study was isolated from infected patients at the Biosafety Level 3 (BSL-3) laboratory at the Shanghai Medical College, Fudan University (Wu et al., 2020b). The SARS-CoV-2 virus was propagated in Vero-E6 cells. Concentrated virus stock was aliquoted and stored at liquid nitrogen. One aliquot of cell line-passaged authentic SARS-CoV-2 virus, originally launched from patient serum and stored at -80°C, was thawed for *in vitro* cell infection experiments.

Bacteria

E. coli Trans5α (TransGen Biotech) were cultured at 37°C with shaking at 230 rpm.

METHOD DETAILS

Collection of human samples

Samples of peripheral blood were collected from SARS-CoV-2 patients at the Zhoushan Hospital in Zhejiang province. Serum samples were heat inactivated for 60 minutes at 56°C, separated by centrifugation of coagulated whole blood, and aliquoted for storage at -80°C. After a 400 mL blood draw from donor #16, human peripheral blood mononuclear cells (PBMCs) were isolated using a cell separation tube with frit barrier. The isolated PBMCs were resuspended in 90% heat-inactivated FBS supplemented with 10% dimethylsulfoxide (DMSO) and cryopreserved in liquid nitrogen.

Antibodies

All the cloned human monoclonal antibodies, their GRLR version, and the previously reported monoclonal antibody CR3022 (ter Meulen et al., 2006) were prepared by transient transfection of mammalian HEK293F cells as previously reported (Wu et al., 2020b).

ELISA

The ELISA binding of serum samples or purified IgG antibody fractions from serum samples or recombinant IgG antibodies against SARS-CoV-2 proteins, including S-ECD-, RBD-, S1-, S2-, and N-proteins (see details in Key resources table) was measured as previously reported (Wang et al., 2020b). Briefly, ELISA plates were first coated with 10 $\mu\text{g/ml}$ of antigen in phosphate buffered saline (PBS) overnight at 4°C, and then blocked with 2% bovine serum albumin (BSA) in PBS. The serum or 1st antibody was serially diluted 1:3 in PBS (maximum concentration, 1:10 for serum, 10 $\mu\text{g/ml}$ for monoclonals) for eight dilutions in total, and added for incubation for one hour at room temperature. Visualization was with HRP-conjugated goat anti-human IgG (Thermo Fisher Scientific) or HRP-conjugated mouse anti-human IgG Fab (GenScript). The area under the curve (AUC) was calculated for each antibody by analysis using PRISM software to evaluate the antigen-binding capacity. ELISA assays using RBD mutants was performed as described above except coating RBD-Fc at a concentration of 2 $\mu\text{g/ml}$, and using wild-type RBD as a reference for normalization.

Competition ELISA

Competition ELISAs were performed as described previously (Wang et al., 2020b). Briefly, plates were coated with 2 $\mu\text{g/ml}$ SARS-CoV-2 RBD or 2 $\mu\text{g/ml}$ SARS-CoV-2 S-ECD and incubated with 15 $\mu\text{g/ml}$ 1st blocking antibody/proteins (60 $\mu\text{g/ml}$ for antibody CR3022) for two hours. Biotinylated 2nd antibodies/proteins (0.25 $\mu\text{g/ml}$) (15 $\mu\text{g/ml}$ for antibody CR3022) were directly added for 30 minutes at room temperature. Detection was performed with streptavidin-HRP (BD Biosciences). PBS buffer substituted for the 1st blocking antibody was used as a reference for normalization, while the anti-HBs antibody H004 (Wang et al., 2020b), which could not block the binding of the 2nd antibodies, served as a negative control.

Preparation of SARS-CoV-2 and SARS-CoV-1 pseudotyped virus

The pseudotyped viruses were produced as previously reported (Xia et al., 2020a). Briefly, plasmids pNL4-3.luc.RE (the luciferase reporter-expressing HIV-1 backbone) and pcDNA3.1-SARS-CoV-1-S/pcDNA3.1-SARS-CoV-2-S (encoding for the S-protein of SARS-CoV-1 or SARS-CoV-2) were co-transfected into HEK293T cells using the transfection reagent VigiFect (Vigorous Biotechnology, Beijing). The supernatant containing the released pseudotyped particles was harvested at 72 hours post-transfection. After centrifugation, the supernatant was collected, aliquoted, and frozen at -80°C . The production of the SARS-CoV-2 pseudovirus mutants was performed as described above except using the plasmids of pcDNA3.1-SARS-CoV-2 with the corresponding mutations (V341I, F342L, V367F, R408I, A435S, G476S, and V483A) in the S-protein (Ou et al., 2020). These plasmids were constructed using the plasmid of pcDNA3.1-SARS-CoV-2-S as a template by a site-directed mutation kit (Yeasen Biotech, Shanghai).

In vitro neutralization assay by pseudotyped SARS-CoV-1 and -2 viruses

In vitro SARS-CoV-1 and SARS-CoV-2 pseudovirus infection was performed as previously described (Xia et al., 2020a). Briefly, 1×10^4 /well Huh-7 cells were seeded in 96-well plates in DMEM supplemented with 10% FBS. The seeded cells were cultured for an additional eight hours before infection. To quantitate the neutralization capacity, the human serum (maximum concentration, 1:20), polyclonal antibodies purified from human serum (maximum concentration, 50 $\mu\text{g/ml}$), or monoclonal antibodies (maximum concentration, 10 or 1 or 0.625 $\mu\text{g/ml}$) was serially diluted 1:2 in DMEM medium for nine dilutions in total. Subsequently, the diluted antibodies or serum samples were incubated with SARS-CoV-1 or -2 pseudoviruses for 30 minutes at 37°C before added onto Huh-7 cells for infection. For the neutralization blocking experiments, different antigens (RBD, S1, S2 or S-ECD proteins) were incubated at different concentrations, respectively, with 5 $\mu\text{g/ml}$ purified IgG from donor #16 for one hour at 37°C before incubation with SARS-CoV-2 pseudovirus. After incubation for half an hour, the mixture was finally added to the Huh-7 cells for infection. After incubation for 12 hours, the supernatant was replaced with fresh DMEM medium supplemented with 2% FBS. The cell supernatant was removed after culture for further 48 hours, and the cells were lysed for luciferase activity measurement using a Firefly Luciferase Assay Kit (Promega) and luminometer according to the manufacturer's instructions.

The absolute luciferase values were measured and the relative values were calculated by normalizing to the virus-only control well in the same lane. For example, the absolute luciferase value in a pseudovirus-only control well (considered as reference) was 5×10^4 , while adding one neutralizing serum sample might reduce this to 1×10^4 . Therefore, the normalized luciferase values were calculated as 100% in the pseudovirus-only control and 20% for this neutralizing serum. Since many aspects, such as pseudovirus concentration, cultured cell concentration, status of the cells, immunofluorescence reading, and etc., varied dramatically between different plates and different tests, normalization is necessary for combining data for comparison. For the serum neutralization assays (Figures 1F and 1G), the reciprocal of the serum dilution that resulted in 50% inhibition compared with pseudovirus alone was reported as the 50% neutralization titer (NT_{50}).

In vitro neutralization assay by authentic SARS-CoV-2 virus

In vitro authentic SARS-CoV-2 neutralization assay was performed using Vero-E6 as previously reported (Chi et al., 2020). Briefly, 1×10^4 /well Vero-E6 cells were seeded in 96-well plates. After culture for 24 hours, the 1:4 serially diluted antibodies (maximum

concentration, 5 $\mu\text{g}/\text{ml}$) were mixed with 0.1 MOI (multiplicity of infection) authentic SARS-CoV-2 virus and incubated at 37°C for 30 minutes. This mixture was subsequently added into the cultured Vero-E6 cells. The supernatants were collected after further culture for two days for quantitative reverse transcription PCR and the cells were analyzed by immunofluorescence.

For immunofluorescence, the cells were fixed in 4% paraformaldehyde in PBS for 20 minutes, washed with PBS and permeabilized with 0.1% Triton X-100 in PBS at room temperature. After blocking with 3% BSA, the cells were incubated with anti-N polyclonal antibody (Gu et al., 2020) at a dilution of 1:1000 overnight at 4°C and visualized with donkey anti-mouse IgG Alexa Fluor 488 (Thermo Fisher Scientific). Nuclei were stained with DAPI. Cells were imaged using an Eclipse Ti-S inverted fluorescence microscopy (Nikon).

For quantitative reverse transcription PCR, the viral RNA was extracted from the collected supernatant using Trizol LS (Thermo Fisher Scientific) and used as templates for quantitative PCR analysis by One-Step PrimeScrip RT-PCR Kit (Takara) following the manufacturer's instructions. The primers and probe used were listed in Table S2. The PCR amplicon by SARS-CoV-2-N-F and SARS-CoV-2-N-R primers was inserted into pUC57 plasmid for standard curve generation. The program of the quantitative reverse transcription PCR was performed using the Mastercycler ep realplex Real-time PCR System (Eppendorf) as followed: 95°C 5 minutes; 40 cycles of 95°C 10 s, 50°C 30 s, 72°C 30 s.

In vitro assay to detect antibody-dependent viral entry

In vitro SARS-CoV-2 pseudovirus ADE assays was performed using Raji cells as previously reported (Jaume et al., 2011). Briefly, 3×10^4 Raji cells were seeded in each well of 96-well plates coated with 0.01% poly-L-lysine in PBS and cultured for 24 hours. The antibodies were serially diluted 1:2 (maximum concentration, 100 $\mu\text{g}/\text{ml}$) in RPMI 1640 for nine dilutions in total, and were incubated with the SARS-CoV-2 pseudovirus for 30 minutes. The mixture was applied onto the Raji cells and cultured for 60 hours. The measurement of luciferase activity was performed as described above using a Firefly Luciferase Assay Kit (Promega). The absolute luciferase activity values from all the wells were normalized to the luciferase activity value obtained with 2 $\mu\text{g}/\text{ml}$ of antibody XG043 and expressed as the fold change in luciferase activity. Two replicates of XG043 (2 $\mu\text{g}/\text{ml}$) were performed on each plate and the average luciferase activity value of these two replicates was considered as reference (100% relative luciferase activity, the dotted lines in Figures 6A, 6D, and 6E; Figure S6B). Since many factors (virus concentration, cell concentration, immunofluorescence reading, etc.) vary between different plates or different rounds of experiments, normalization is necessary for comparing the luciferase activity values from different plates. The reason for choosing XG043 as the reference is simply because that XG043 was the first identified to induce ADE in our studies.

For the experiment to block the antibody-dependent viral entry, different concentrations of anti-hCD32 (BD Pharmingen) were incubated with the Raji cells for 30 minutes at 37°C. Then, the mixture of 2 $\mu\text{g}/\text{ml}$ antibody XG005 and SARS-CoV-2 pseudovirus was added to the treated Raji cells. The plates were incubated at 37°C for 60 hours before the measurement of luciferase activities as described above.

For *in vitro* Raji cell-dependent ADE assays using authentic SARS-CoV-2 virus, cultured Raji cells were incubated with the mixture of authentic SARS-CoV-2 virus and monoclonal antibodies (final concentration 4 $\mu\text{g}/\text{ml}$), XG038, XG016 and XG005, respectively. After 6, 24 or 48 hours incubation, the Raji cells were collected for RNA extraction and quantitative reverse transcription PCR analysis. SARS-CoV-2 N-protein RNA copy numbers were calculated using a standard curve composed of seven prepared N-protein DNA samples with 10-fold serial dilutions.

Protein production

The codon optimized wild-type cDNA of SARS-CoV-2 receptor-binding domain (RBD) (amino acid 330–530) together with an Avi tag (GLNDIFEAQKIEWHE) was synthesized (GENEWIZ), and cloned into pACgp67 vector with a C-terminal 8 \times His tag for purification. The SARS-CoV-2 RBD was expressed using the Bac-to-Bac baculovirus system. Extracted bacmid DNA was then transfected into Sf9 cells using Cellfectin II Reagent (Invitrogen). The low-titer viruses were harvested and then amplified to generate high-titer virus stock. The supernatant containing the secreted RBD without glycosylation was harvested 72 hours after infection and the RBD protein was captured by Ni-NTA resin (GE Healthcare) and purified. SDS-PAGE analysis revealed over 95% purity of the purified recombinant protein.

For the site-directed mutagenesis and expression of RBD mutants, SARS-CoV-2 RBD fragment (residue 319–541) and its mutants were synthesized (GenScript), fused with the human IgG1 Fc fragment, and cloned into mammal expression vector pSecTag. The plasmid was transfected into HEK Expi293 cells and incubated at 37°C for four days. Supernatant was harvest for further purification by Protein G resin according to the manufacturer's protocol.

Single cell sorting of RBD- or S-ECD-binding memory B cells

S-ECD protein (GenScript) expressed and purified from recombinant baculovirus-infected insect Sf9 cells was chemically biotinylated using EZ-Link Sulfo-NHS-LC-Biotin kit (Thermo Fisher Scientific) as manufacturer's instructions. Avi-tagged RBD expressed in baculovirus-infected insect Sf9 cells and Avi-tagged S-ECD expressed in mammalian HEK293T cells (Kactus Biosystems) were biotinylated using BirA Biotin-Protein Ligase kit (Avidity). The excess of unbound biotin was removed by using Zeba Spin Desalting column (Thermo Fisher Scientific). For each sample, the bait protein-PE and bait protein-APC were prepared by incubating 3 μg of biotinylated RBD or 25 μg of biotinylated S-ECD proteins with streptavidin-PE (eBioscience) or streptavidin-APC (BD Biosciences), respectively.

Purification of B cells, two-fluorescent-dye labeling of bait protein-binding B cells and single cell sorting experiments were performed as previously described (Escolano et al., 2019; Robbiani et al., 2017; Wang et al., 2020b). Briefly, PBMCs thawed and washed with RPMI medium were incubated with CD19 MicroBeads (Miltenyi Biotec) for positive selection of B lymphocytes. Sequential incubation at 4°C with human Fc block (BD Biosciences), bait protein-PE/APC (10 μg/ml for RBD, 60 μg/ml for S-ECD), and anti-CD20-PECy7 (BD Biosciences) was performed, followed by the single-cell sorting of CD20-PECy7⁺ bait protein-PE⁺ bait protein-APC⁺ memory B cells into 96-well plates using a FACSaria II (BD Biosciences). The single-cell sorted B cells were stored at –80°C.

Antibody cloning, sequencing and production

Antibody cloning from the sorted single cells and the production of monoclonal antibodies were done as previously reported (Robbiani et al., 2017; Wang et al., 2020b). The sequences of primers for the 1st/2nd round of nested PCR were listed in Table S2. Amplified PCR products from each single cell were loaded onto 2% agarose gel for electrophoresis and purified for Sanger sequencing. All the sequencing result of heavy and kappa/lambda light chains were analyzed by IMGTV-QUEST (Brochet et al., 2008) and IgBlast (Ye et al., 2013), and the V(D)J gene segment and CDR3 sequences of each antibody were determined. The selected antibodies were subjected to vector construction and antibody expression as previously described (von Boehmer et al., 2016).

Clustering analysis

Relative luciferase activities measured in neutralization or ADE assays or both were used for unsupervised hierarchical clustering analysis with the statistical scripting language R, using log-transformed data, Euclidean correlation coefficients for a distance metric, and ward.D2 clustering. A heatmap and cluster dendrogram tree were created using the Pretty Heatmaps (pheatmap and hclust) R packages.

QUANTIFICATION AND STATISTICAL ANALYSIS

The detailed results of statistical analysis are shown in the Result and Figure Legends. The Shapiro-Wilk test and Fisher's F test were employed to check for normality and homogeneity of variances, respectively, prior to performing the comparison. Student's t test was performed for RBD ELISA (Figure 1A), while Wilcoxon Rank Sum test was used for other ELISAs (Figures 1B–1E) and comparisons of ADE AUC (Figure 7E) due to their non-normal distribution. In order to determine whether there is a statistically significant difference of the ADE AUC and IC₅₀ values of Cluster-X, -Y, and -Z antibodies, the nonparametric test (Dunn's Kruskal-Wallis multiple comparison) was performed (Figures 7B and 7C). Fisher's exact test was performed to assess the statistical significance based on the exact distribution of the frequencies of RBD Group-IV antibodies in three antibody clusters (Figure 7D). Correlation was evaluated by Spearman's rank correlation method (Figures S6E–S6G). The area under the ELISA curves (ELISA AUC) (Figures 1A–1E and 3A–3D), the half-maximal neutralizing titer (NT₅₀) for serum neutralization assays (Figures 1F–1H), the 50% inhibitory concentration (IC₅₀) values calculated for antibody neutralization capacities (Figures 4A, 4F, and 5C), the area under the ADE curve (ADE AUC) (Figure 6C), and enhancing power values (Figure S6D) were calculated in PRISM software as previously reported (Bardina et al., 2017; Robbiani et al., 2019; Wang et al., 2020b).